Resistivity and IP measurements at the Bolmen Tunnel and Ådalsbanan, Sweden

Miriam Cegrell and Jimmy Mårtensson

Examensarbeten i Geologi vid Lunds universitet - Berggrundsgeologi, nr. 231 (30 hskp/ECTS)

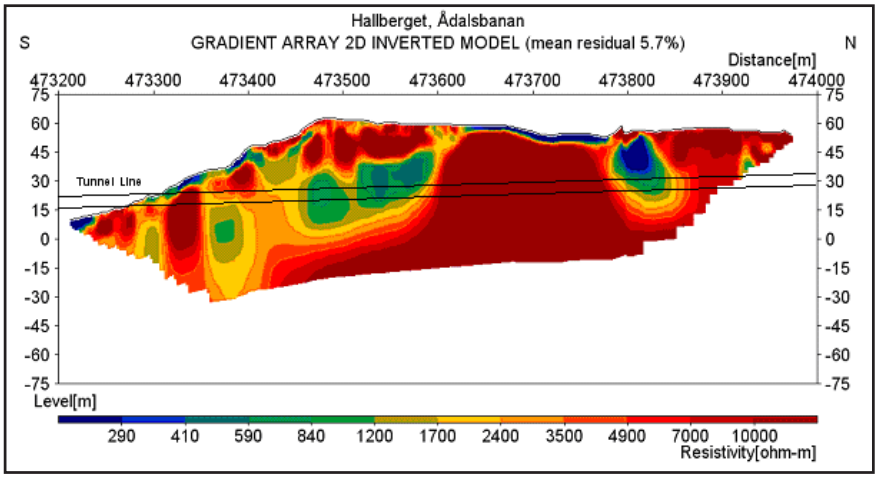

Tillika:
Examensarbete i Teknisk geologi vid Lunds Universitet / LTH

Geologiska institutionen
Centrum för GeoBiosfärsvetenskap
Lunds universitet
2008

Resistivity and IP measurements at the Bolmen Tunnel and Ådalsbanan, Sweden

Master Thesis

Miriam Cegrell
Jimmy Mårtensson

Department of Geology Engineering geology
Lund University
2008

Contents

Cover Picture: Resistivity Section, Hallberget

Preface

The study has been divided as follows:
Miriam Cegrell has been responsible for the results and discussion for Ådalsbanan, chapter 8, 9 and 10.
Jimmy Mårtensson has been responsible for the results and discussion for Bolmen, chapter 6 and 7.
The remaining part of the work has been carried out together by both authors.

Resistivity and IP measurements at the Bolmen Tunnel and Ådalsbanan, Sweden

MIRIAM CEGRELL and JIMMY MÅRTENSSON

Cegrell, M., Mårtensson, J., 2008: Resistivity and IP measurements at the Bolmen Tunnel and Ådalsbanan, Sweden. *Examensarbeten i geologi vid Lunds universitet*, Nr. 231, 46 pp. 30 hp.

Abstract: In all tunnel construction projects geophysical methods are important as a foundation for engineering geological conceptual models. Detailed information about the condition and the physical properties of rocks at depth is desirable, and geophysical methods have the potential to exploit these properties. This work is based on geophysical investigations with focus on the geoelectrical methods. The methods are direct current (DC) resistivity and induced polarisation (IP). The use of the continuous vertical electrical sounding (CVES) gives continuous data in a time and cost efficient way. The methods have been tested at two tunnel investigation sites in Sweden, at the Bolmen tunnel and Ådalsbanan. Complementary magnetic and VLF (Very Low Frequency) measurements has also been carried out. Pre-investigations of tunnelling construction projects commonly include core drilling. The resistivity and IP methods provide significant geological information and by including these methods at an initial stage, the selection of drilling site can be optimized. By combining different geophysical methods with drilling a more reliable model can be compiled. The resistivity method is based on the fact that each rock has a specific physical character. The physical property of the rock can then be interpreted in terms of geological properties and in some cases even allow an assessment of the rock mass quality. The main purpose in this work was to estimate the applicability and the limitations of these methods used for pre-investigation in tunnel construction projects. This material includes geological interpretations and estimations of the quality of the rock based on geoelectrical methods. With the resistivity method several low resistive zones were detected and interpreted as weakness zones. Many of these were verified by data from earlier tunnel investigations. The IP method gave information about the character (e.g. water and clay content) of the fracture zones and served as a complement to the resistivity method. These methods provided general information, from which a geological model was estimated. The results show that the resistivity and IP are useful methods in pre-investigation for sub-surface tunnel constructions.

Keywords: Resistivity, induced polarisation (IP), geophysics, geology, Bolmen, Ådalsbanan.

Miriam Cegrell, Department of Geology, GeoBiosphere Science Centre, Lund University, Sölvegatan 12, SE-223 62 Lund, Sweden. E-mail: miriam.cegrell.389@student.lu.se

Jimmy Mårtensson, Department of Geology, GeoBiosphere Science Centre, Lund University, Sölvegatan 12, SE-223 62 Lund, Sweden. E-mail: jimmy.martensson.590@student.lu.se

Resistivitet och IP mätningar längs Bolmen tunneln och Ådalsbanan, Sverige

MIRIAM CEGRELL och JIMMY MÅRTENSSON

Cegrell, M., Mårtensson, J., 2008: Resistivitet och IP mätningar längs Bolmen tunneln och Ådalsbanan, Sverige. *Examensarbeten i geologi vid Lunds universitet*, Nr. 231, 46 sid. 30 hp.

Sammanfattning: Geofysiska metoder används vid alla tunnelbyggnadsprojekt då geotekniska beskrivningar och modeller baseras på resultat från dessa. Detaljerade redogörelser för markförhållanden och information om djupet till berggrunden är av intresse, och med geofysiska metoder kan dessa parametrar utvärderas. Detta arbete är baserat på geofysiska undersökningar med fokus på de geoelektriska metoderna. Metoderna som använts är DC (direct current) resistivitet och inducerad polarisation (Induced Polarisation, IP). CVES (Continous Vertical Electrical Sounding) är en kostnads- och tidseffektiv resistivitets-metod som ger kontinuerlig data. Dessa metoder har testats på undersökningsområden belägna ovanför två tunnlar i Sverige, Bolmentunneln och Ådalsbanan. Komplimenterande mätningar med VLF (Very Low Frequency) och magnetometer har även utförts. Förundersökningarna till tunnelprojekt innefattar ofta kärnborrning. Resistivitet och IP metoden ger viktig geologisk information och genom att i ett tidigt skede inkludera dessa metoder, kan en bedömning av det mest optimala läget för borrningen göras. Användandet av flera geofysiska metoder tillsammans med borrningar, ökar tillförlitligheten i den framtagna modell som visar markens uppbyggnad. Resistivitetsmetoden bygger på att man kan särskilja olika bergarter då deras fysiska egenskaper skiljer sig. En bergarts fysiska egenskaper kan kopplas till dess geologiska karaktär och i vissa fall kan även en bedömning av bergets kvalitet göras. Syftet med denna studie har varit att utvärdera metodernas användbarhet och eventuella begränsningar i samband med förundersökningar till tunnelprojekt. Detta arbete innefattar geologiska tolkningar och utvärderingar av bergkvalitén som baserats på resultaten från de geoelektriska metoderna. Med resistivitetsmetoden detekterades flera lågresistiva zoner som tolkades som svaghetszoner. Förekomsten av flertalet svaghetszoner kunde verifieras av data från tidigare tunnelundersökningar. IP-metoden gav information om sprickzonernas karaktär (såsom förekomst av vittring och lerinnehåll) och har i detta arbete fungerat som ett komplement till resistivitetsmetoden. Dessa metoder ger övergripande information om geologin och utifrån denna kan en geologisk modell tas fram. Resultaten visar att resistivitets- och IP-metoden är användbara metoder i förundersökningar för konstruktionsprojekt av bergtunnlar.

Nyckelord: Resistivitet, inducerad polarisation (IP), geofysik, geologi, Bolmen, Ådalsbanan.

Miriam Cegrell, Geologiska Institutionen, Centrum för GeoBiosfärsvetenskap, Lunds Universitet, Sölvegatan 12, SE-223 62 Lund, Sverige. E-post: miriam.cegrell.389@student.lu.se

Jimmy Mårtensson, Geologiska Institutionen, Centrum för GeoBiosfärsvetenskap, Lunds Universitet, Sölvegatan 12, SE-223 62 Lund, Sverige. E-post: jimmy.martensson.590@student.lu.se

1 Introduction

Limited information about the ground conditions is considered to be a major risk factor during subsurface constructions that may result in delays and unexpected expenses (Danielsen 2007). Careful investigations of the geology combined with geophysical measurements at the construction site and surrounding areas could potentially prevent such situations to arise.

A major technical problem in tunnel constructions is often the leakage of water through cracks and fractures in rocks (Cesano et al 2000). Leakages through zones with clay minerals are especially problematic since many clays show an active swelling in contact with water. This in turn may result in a loss of stability which requires extensive rock-support (Olofsson 1991). Tunnelling through rock of poor quality may require pregrouting and other actions to prevent the water seepage that may raise the cost of the project significantly (Bäckblom & Stanfors 1986). According to a statistical analysis made by Cesano et al. (2000), significant leakage is of particular concern in areas with direct hydraulic contact between the fractured bedrock and the soil-aquifers. In Sweden, this normally occurs in areas with thick layers of soil, for instance in valleys where loose sediments usually overlie fractured bedrock. This situation may result in a lowering of the groundwater level in the surrounding soil layers, which in turn may effect the local environment (Axelsson & Follin 2000).

In technical investigations, core drilling is often used to provide qualitative information of different rock lithologies. Since the information obtained from a drill core is restricted to a point source a brief geologic overview of the investigation area is necessary in order to determine the most appropriate site for drilling (Dahlin et al. 1996).

Geophysical measurements can give continuous information about the geological environment at the construction site. The resistivity method can contribute information about the ground conditions at an investigated site. When interpreting the results from geophysical measurements knowledge about the geology is of great importance. Therefore a geological description of all investigation sites will be presented in this study. Rearmost in the work a useful dictionary has been appended.

This work is based on geophysical investigations with focus on the geoelectrical methods Direct Current (DC) resistivity and Induced Polarisation (IP). During recent years these methods have been continuously refined, though a number of limitations still remain. Complementary geophysical measurements with magnetometer and VLF have also been performed. Field measurements have been carried out above the Bolmen tunnel and along two of the planned tunnels for Ådalsbanan (Fig. 1).

The Bolmen tunnel is an existing water tunnel that distributes water from the lake Bolmen in Småland that supplies a large amount of water to the county of Scania. The Bolmen tunnel extends over 80 km and was constructed between the years 1975 and 1985. The geology in this area is very complex, which aggravated the construction work of the tunnel. In recent time the tunnel has collapsed several times. Most likely these events are linked to fracture zones abundant in the bedrock. Additional information about the fracture zones and their connection to the tunnel is therefore of interest.

Ådalsbanan is an extended railway line in Västernorrland. At present, extensive work including restoration of Ådalsbanan is taking place. This involves construction of several new tunnels of which two have been investigated in this work. The bedrock is made up of various lithologies with different geotechnical properties. A better insight of structures in the subsurface is therefore desirable.

The aim of this study is to:

- evaluate the applicability and limitations of the resistivity and IP methods as tools in pre-investigation of tunnel constructions,
- outline the geology and present an interpretation model for the investigation sites,
- estimate the depth-to-bedrock and the occurrence of fracture zones at the investigated areas.

This work has been accomplished with support from Sydvatten AB and Banverket projektering. Provided information and documentation have been used during the work and in the final interpretations. Equipment and logistics has been supported from the faculty of Engineering Geology. The work has been economically supported by SveBeFo (Svensk Bergteknisk Forskning) and SBUF (Svenska Byggbranchens Utvecklingsfond) via the project; The Applicability of Geoelectrical Imaging as a Tool for Design and Construction in Rock.

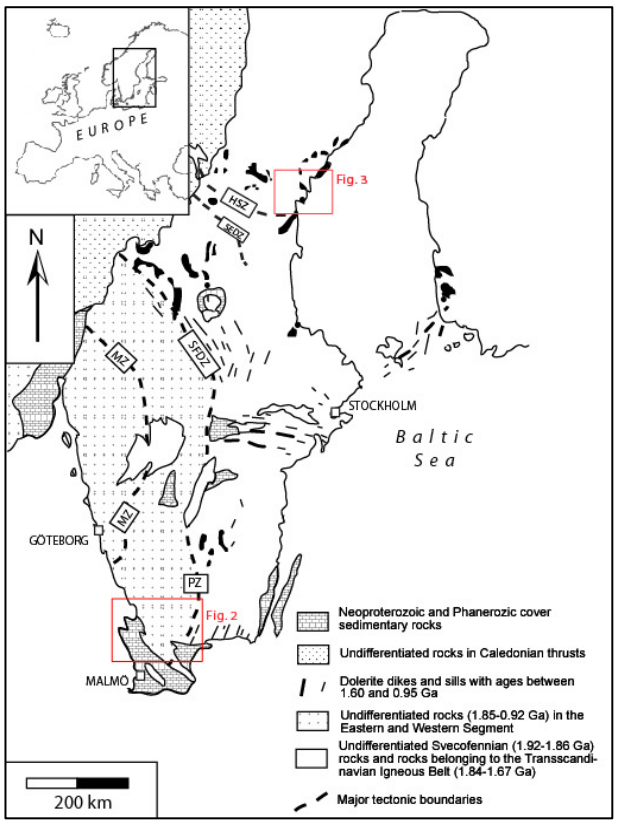

Fig.1: Geological map over Sweden showing the investigated areas (modified from Söderlund et al. 2005). PZ=Protogine Zone, SFDZ=Sveconorwegian Frontal Deformation Zone, MZ=Mylonite Zone, HSZ=Hassela Zone, SEDZ= Storsjön-Edsbyn zone. Red frames depict site investigation areas shown in Fig. 2 (the Bolmen tunnel) and Fig. 3 (Ådalsbanan).

2 Geology at the Bolmen tunnel

2.1 Regional Geology

The Bolmen tunnel is located in the Eastern Segment of the 1.03-0.95 Ga Sveconorwegian orogen (Fig. 1). The Eastern Segment is delimited by two major deformation zones, the Protogine Zone in the east and the Mylonite Zones in the west (Andréasson & Rodhe 1990). The crystalline basement is dominated by more or less penetratively deformed rocks metamorphosed under high-grade (amphibolite to granulite) conditions (Andersson et al. 1999; Möller et al. 2007). The granitic gneisses are usually interpreted to represent reworked equivalents of granites and supracrustal rocks of the 1.81-1.65 Ga Transscandinavian Igneous Belt (TIB) that dominates the bedrock in southern Sweden (Bingen et al. 2008). The origin of TIB is not fully understood but most geologists favour long-lived subduction of oceanic crust in the west, similar to present processes along the western South America (cf. Åhäll & Connelly 2008). During the 1.47-1.43 Ga Hallandian-Danopolonian event (Bogdanova et al. 2001), mantle generated orogenic magmatism led to intrusion of granodioritic and charnokitic rocks in southwestern Sweden at ~1.47-1.45 Ga (Brander & Söderlund 2008). This event was associated with high-grade metamorphism (including anatexis), veining and local deformation in southern Sweden (Möller et al. 2007). The following episode at ca. 1.2 Ga was characterized by tensional magmatism along the Protogine Zone that caused dyking of diabase dykes and emplacement of syenite, granite and ultramafic plutons. Examples are the ca. 1203 Ma Taberg body (Larsson & Söderlund 2005), and the 1220 Ma Vaggeryd syenite (Söderlund & Ask 2006). During the Sveconorwegian orogeny (ca. 1.03-0.95 Ga), rocks west of the Protogine Zone was reworked under high-grade metamorphic conditions (Johansson et al. 2001). These rocks were uplifted and eroded ~0.95-0.90 Ga ago as the Sveconorwegian mountain range denudated (Möller & Söderlund 1997).

2.2 Local geology

A great part of the bedrock that was drilled during construction of the Bolmen tunnel is made up of granite gneisses, with subordinate mafic amphibolites. Quartz and feldspar veins are common as the result of veining and partial melting (Wik et al. 2006).

Common features in weak zones are brecciation and mylonitization. The frequency and complexity of deformation zones is likely to manifest multiple tectonic events throughout the Protorezoic and, possibly also, the Phanerozoic. The formation of mylonites commonly involves successive stages of deformation, recovery and recrystallization. During deformation, pressure solution may contribute to fabric development, whereas brecciation is basically mechanical in nature (Gierup et al. 1999b).

2.3 Tectonic features and quaternary deposits

Generally, the northern part of the Bolmen tunnel is characterized by fracture and fault zones typically having NNE trends, while the southern part is dominated by WNW oriented fracture zones (Didriksson & Isander 1995).

The boundary between the Eastern Segment gneisses and the relatively undeformed granitoids of the Transscandinavian Igneous Belt is the major intraplate tectonic zone, known as the Protogine Zone (Fig.1). The fractures in the northern part probably manifest a western extension of Protogine Zone deformation since they typically have the same orientation. In the south, the tunnel intersects multiple brittle WNW-trending fractures of the Tornquist Zone (Johansson et al. 1992). This zone extends from the Black Sea to the North Sea, and is the border between the Baltic Shield and the East European Craton (Freden 2002). Repeated movements along fracture zones during the Mesozoic gave rise to the horst-graben system in Scania. Hundreds of dolerite dykes, dated at ca. 300 Ma (Bergelin, Lund Univ., pers. comm.. 2008), trend parallel to the Tornquist Zone in Scania. The average strike of faults and dykes is WNW with a dip to the

SW that is moderately steep.

The quaternary deposits have a thickness that ranges between five and ten metres and cover the tunnel completely. The bedrock above Bolmen tunnel is covered by relatively thin and sandy till that usually follows the bedrock surface. Till formations as hummocky moraine has a large distribution, especially in the southern part of Kronoberg (Gierup et al 1999a & b). Till is usually a heterogeneous soil with zones of low conductivity and are therefore less important in the hydrogeological contexts (Cesano et al. 2000). Glaciofluvial formations (e.g. eskers) and peat, with high conductivity are found in the whole region and are commonly located in low areas as valleys. Extensive glaciofluvial sediments are preferentially found in the valley of the Lagan River, close to the Bolmen tunnel (Gierup 1999b).

2.4 Tunnel documentation

In 1983, when the work of the Bolmen tunnel was in full progress, a research project including scientist from different departments of technical universities in Sweden was launched. The project was concentrated to a small part of the tunnel in an area near the village Staverhult, where the results of former investigations had indicated the occurrence of extensive fracture zones. For this reason the tunnel route was moved to an area of better rock quality (Bäckblom & Stanfors 1986).

In the Bolmen tunnel, most of the leaking fractures are found in the northernmost (0-25 km) part (Fig.2) (Cesano et al 2000). Before the tunnel was filled with water a lowering of the groundwater level was documented in the Staverhult area (Axelsson & Follin 2000). A fen close to the tunnel was dehydrated and chemical analyses of the water indicated a drainage from the overlying aquifer into the bedrock. When the tunnel was re-filled with water, the groundwater levels in some places became higher than before, leading to oversaturation of water in the soils.

Collapses due to swelling clays has occurred twice (in 1986 and 1995) in the Bolmen tunnel. In 1995, the failure was located to a section with altered bedrock under the Lagan river. Although the tunnel in this part had been reinforced, the affect of swelling of zones eventually caused the tunnel to collapse (Didriksson & Isander 1995).

The Bolmen tunnel penetrates entirely through crystalline rocks. Geological mapping was carried out continuously from the start of blasting of the tunnel in 1975 up to the time of its completion in 1985. According to geological documents, granitic gneisses are the dominating rock type. Numerous bodies of a more unstratified granitoid type of rock (gneiss-granite) dominate the northern half of the tunnel. All metamorphosed mafic rocks were classified as amphibolite. These occur in the form of dykes, massive or thin layers and banks along the entire length of the tunnel, but to a varying extent (Wik et al. 2006). In a limited area in the northern part of the tunnel, a swarm of decimetre wide amphibolite bands are present; they often occur in conjunction with the most serious altered zones (Stanfors 1987).

During construction of the Bolmen tunnel, site investigations were intensified in areas where extensive faulting was suspected (Bäckblom & Stanfors 1986), e.g. in low land areas (Stanfors 1987). From Lake Bolmen, the most prominent zones of weakness (see Fig. 2), were found adjacent to the valley of the Torpaån river (1), the Stavehult area (2), the valley of the Lagan river (3), the area between Markaryd and Lake Kraxasjön (4), the Slättsjö area (5), the valleys of the rivers Perstorpsbäcken (6) and Ybbarpsån (7). Because the tunnel intercects these fractures zones at relatively low angles their exposures may reach as much as a kilometre within the tunnel (Stanfors 1987). Brecciation and mylonization are common in these weakness zones and developed both in the ductile and brittle

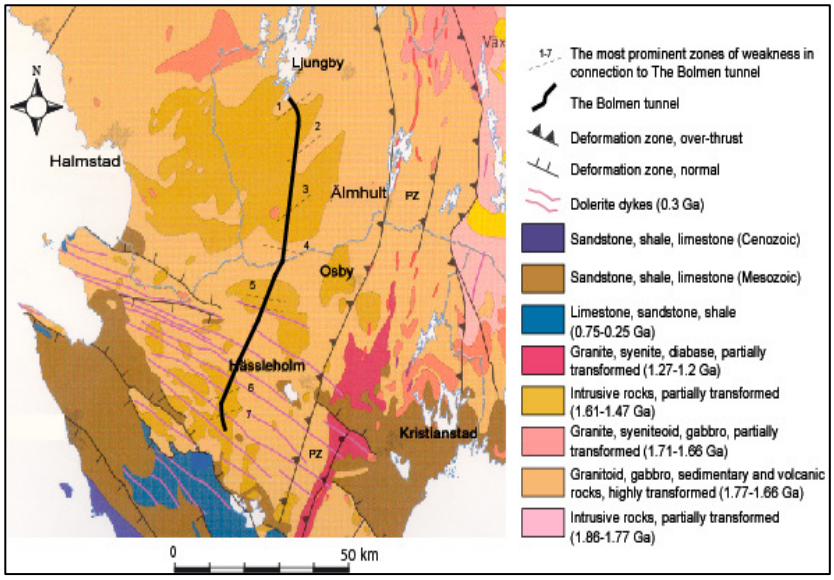

Fig. 2 Map over the regional geology in the area of the Bolmen tunnel (modified map. Bergman et al. 2004).

regimes.
In Scania, the tunnel intersects a large number of dolerite dykes and fractures of the Sorgenfrei-Tornquist zone (see 2.3). For instance, the last 30 km of the tunnel goes through about 120 dolerite dykes of which a third are more than 15 m wide (Gierup et al. 1999a). In a section of the tunnel south of the Slättsjö Zone, complications were encountered during the construction work, presumably related to dense interlaying by amphibolite and gneiss.

3 Geology at Ådalsbanan

3.1 Regional geology

The Ådalsbanan is located in Västernorrland in the central part of Sweden (Fig. 3), in the region between the ore rich provinces of Bergslagen and the Skellefteå field. The major part is made up of Paleoproterozoic (1.96-1.82 Ga) bedrock that was formed during the Svecofennian orogen. At that time, large amounts of sediments and volcanic rocks were accumulated (Lundqvist et al. 1990) in a basin (the Bothnian basin) located between the island arcs of Bergslagen and Skellefteå (Nilsson et al. 2006). The Svecofennian was characterised by frequent volcanic arc-style eruptions with lavas and tuffs dominated by mafic compositions. Early intrusive rocks are dominated by metagranite and metagranodiorite, which are most frequent in the southern part of the region. Sedimentary and volcanic rocks accumulated in the Bothnian basin and were later intruded by plutonic rocks of tonalitic to granitic composition with subordinate gabbro and diorite. During compression and folding the primary layers became tilted, sometimes to an almost upright position. The rocks were exposed to high temperatures and low to moderate pressures, resulting in extensive metamorphism. Parts of the rocks started to melt (especially sediments) and therefore migmatites are common in the region (Lundqvist et al. 1990). During the final phase of the Svecofennian orogeny granitoids of Härnögranite type (1.82-1.84 Ga) were emplaced (Nilsson et al. 2006). The Härnögranite has both muscovite and biotite and is commonly associated with pegmatites, which indicates that these magmas were rich in volatile elements (Nilsson et al. 2006). Most of the strongly reworked rocks have been mapped and classified as metagreywackes. Veins are common and only sparsely primary features are preserved, e.g. sandy and clayey layers. Lenses of skarn occur both parallel and oblique to the foliation. The skarn was formed during transformation of dense carbonate. A few fine grained amphibolite dykes also appear in the area (Nilsson et al. 2006). Dolerite sills and dykes are abundant in the region. The majority of these belong to the Central Scandinavian Dolerite Group, recently dated to ca 1.26-1.25 Ga (Söderlund et al. 2005). These rocks display an ophitic texture and are fine- to medium- grained. Studies of the magnetic susceptibility anisotropy (AMS) and palaeomagnetism indicate that the flow direction of mafic magma was towards the southeast (Lundquist et al. 1990). The Alnö complex, dated at ca. 550 Ma (Andersen 1996), comprises alkaline and carbonaceous rocks, called carbonatite- and Alnöit dykes. The complex consists of one main intrusion and four minor satellite intrusions, whereas all except one can be found on land. Dykes that are associated with the Alnö complex also exists in the surrounding area near Sundsvall. Many dykes have been strongly affected by weathering. The mineral content of the Alnö carbonatites varies but they all have the same main composition (Nilsson et al. 2006). The rocks consist of mica and magnetite and sometimes pyroxenes and amphibole, in a fine grained ma-

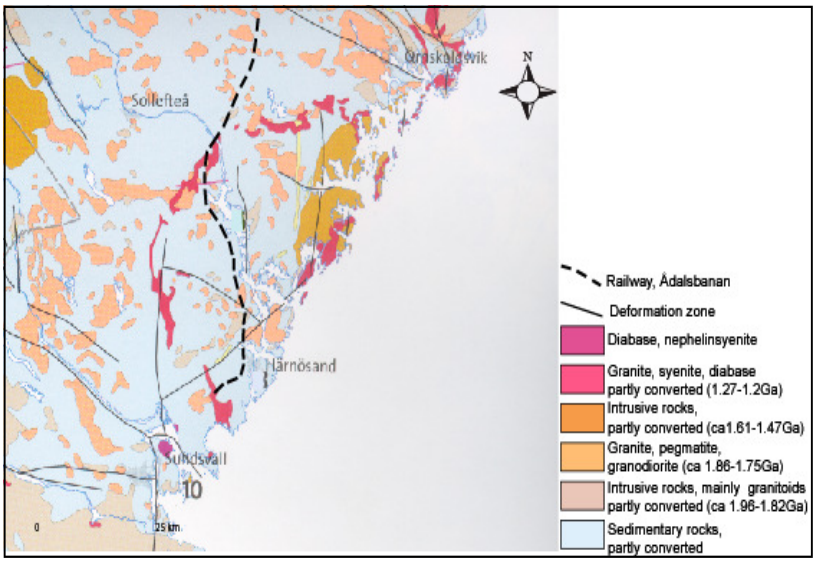

Fig. 3 Geological map showing a part of Ådalsbanan in Västernorrland County (modified map. Bergman et al. 2004).

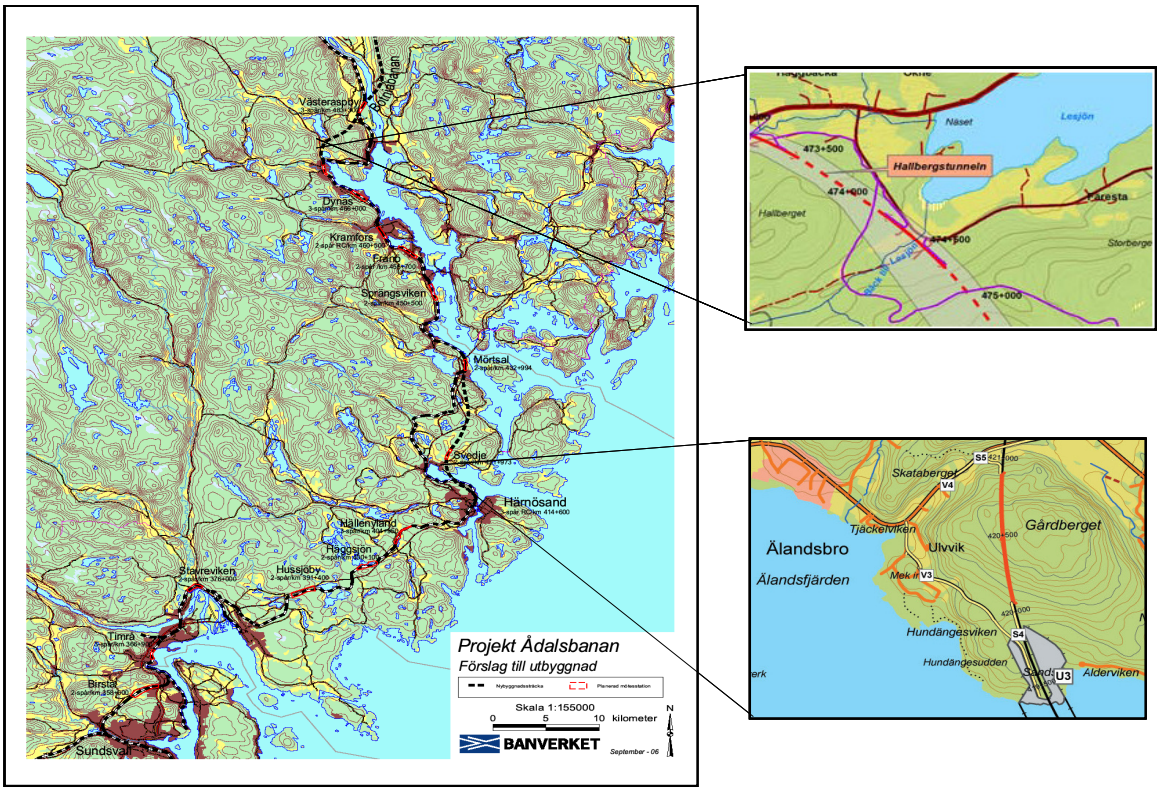

Fig. 4 Map over the investigated areas Hallberget and Gårdsberget at Ådalsbanan (modified map, Banverket 2008)

trix that among other include calcite, magnetite and apatite (Lundquist et al. 1990). The locations of the sites that have been investigated is shown in Fig. 4.

3.2 Tectonic features and quaternary deposits

In Västernorrland, four main directions for the regional fracture zones exist. The inland is dominated by S, NW- and W-trending directions while coastal zones are characterized by NNE orientations (Antal et al 1998).

One of the more prominent shear zones is the Storsjön-Edsbyn zone (SEDZ), southwest of Ånge in the southwestern part of the region (Fig. 1). The SEDZ is 10-20 km wide and 300 km long and comprises various kinds of mylonites. North to the SEDZ another regional zone called the Hassela zone (HSZ) is found (Fig. 1, 3). This zone is a steep WNW- to NW striking dextral shear zones formed under wrench conditions (Högdahl & Sjöström 2001). The ductile NW-SE trending shear zones are the oldest deformation zones in Västernorrland formed during the Svecofennian at depths of 10 to 15 km. Many fracture zones seem to follow the plastic structures, which indicate that reactivation occurred under brittle conditions (≤ ca. 10 km). Younger, N-trending fracture zones cut older deformation zones (Antal et al. 1998).

The occurrences of quaternary deposits in Västernorrland are primarily based on mapping by the Swedish geological survey (Antal et al 1998). The soils in the region are remnants from the last deglaciation. However, in many places the ordinary till overlies an older dark and clayish till that is believed to originate from the last interstadial. The rocks are generally widely exposed along the coast, especially in the areas under the highest coastline (HK) due to relatively rapid isostatic uplift in postglacial time. In the areas under HK the till is absent and most of the previous glacial soils has eroded away, or reworked to form littoral sediments. The littoral sediments are found in exposed areas next under HK and near the coast. Above the HK, the rock exposure is poor and the sandy till has a wide distribution. The thickness of the soil varies but is thickest in the river valleys, reaching depths of 40 to 60 m. Outside the valleys the depths are generally less than 10 m (Antal et al. 1998). Glaciofluvial sediments as sand and gravel overlay the till and are mainly concentrated to large valleys where they build up various types of landforms e.g. eskers and delta complexes (especially close to the HK). Fine-grained sediments like glacial clay and silt were deposited by meltwater from the receding glacier and are common in low land areas. The organic soils are dominated by peat. Peat-lands like fen, bogs and mires are common in the western and northern parts of the county (Antal et al. 1998).

4. Geophysical methods

4.1 Resistivity

Electrical resistivity methods were developed in the early 1900s and have become widely used since the

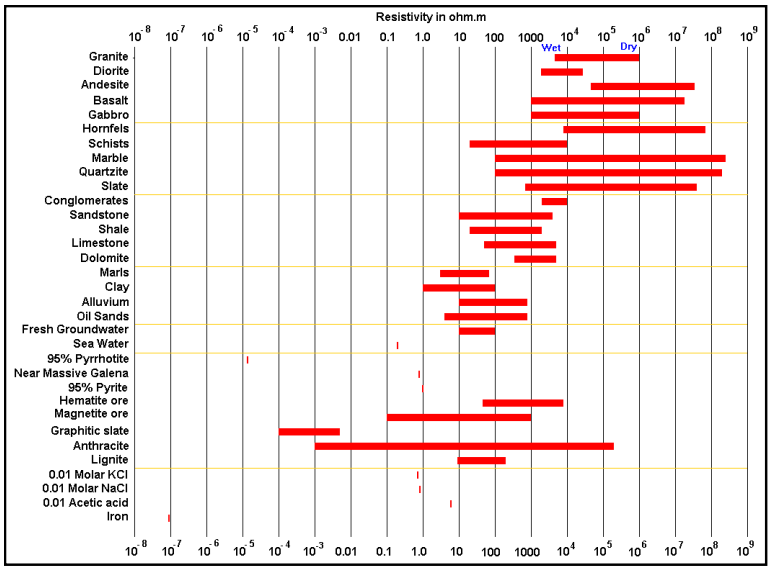

Fig. 5 Resistivities of some common rocks, minerals and chemicals (Loke 1997).

1970s, primarily due to improved prestanda of computers necessary to process the large amount of analytical data inherent in these methods (Reynolds 1997). Electrical resistivity surveys are used in hydrogeological, mining and geotechnical investigations and, more recently, in environmental studies (Loke 2003).

The electrical resistance of a material is usually expressed in terms of its resistivity. It is important to note that resistance is a measure of the degree to which an object opposes an electric current through it, whereas resistivity is a material property that is a measure of how strongly a material opposes the flow of an electric current. Resistivity depicts the ability of a material to act as an isolator (Jeppsson 2006).

The electrical conduction in most rocks is essentially electrolytic. The reason is that most minerals and rocks (except metallic ores and clay minerals) are isolators, and electrical currents are mainly conducted through water hosted in pores and fissures (Sharma 1976).

There are several parameters that affect the resistivity of a rock e.g. porosity, the degree of water saturation in the pores, the resistivity of the fluid, mineral composition and mineral structure (Jeppsson 2006). Resistivity is therefore an extremely variable parameter, not only between formations but even within a particular formation (Sharma 1976).

The correlation between resistivity and lithology can be illustrated in a classification diagram (Fig. 5). Although there is no general correlation between the lithology and resistivity a broad classification can be made. Difficulties arise because certain resistivity intervals correspond to more than one lithology that sometimes makes the classification of different rocks in definite. Igneous rocks tend to have the highest resistivities, sedimentary rocks tend to be most conductive, largely due to their high pore fluid content whereas metamorphic rocks have intermediate resistivity (Reynolds 1997). For sedimentary rocks, it is important to characterise the resistivity of the interstitial fluid as many sedimentary rocks comprise pores filled with fluids. Archie's Law is an empirical formula that often is used when determining the resistivity of sedimentary rocks. The formula takes into account the porosity, the fraction of the pores containing water and the resistivity of the water (Reynolds 1997).

4.1.1 Theory

The fundamental physical law used in resistivity surveys is Ohm´s Law that governs the flow of a current in the ground. The equation for Ohm´s Law for a current in a continuous medium is given by

$$J = \sigma E \qquad (4.1)$$

in which σ is the conductivity of the medium , J is the current density and E is the electric field intensity (Parasnis 1986). In geophysics the resistivity of a medium is commonly used, which is the reciprocal of the conductivity ($\rho=1/\sigma$). The SI-unit for resistivity is ohm metre (Ωm) and Siemens/metre (S/m) for conductivity (Reynolds 1997). The simplest approach to describe resistivity is to imagine sending a electric current (I) through a short, thin, linear conductor of uniform cross section given by Ohm´s Law as

$$I = -\frac{\delta V}{R} \qquad (4.2)$$

where δV is the potential difference between the ends of the conductor, divided by the resistance of the conductor. The negative term expresses the fact that the current flow moves from high to low potential. The potential difference (p.d) across the ends of the conductor is given by Ohm´s Law;

$$\delta V = RI \qquad (4.3)$$

which gives

$$R = \frac{\delta V}{I} \qquad (4.4)$$

The next step in development of the theory is to clarify how the potential can be measured. The potential at any point in the ground is dependent on the distance to the current electrodes (Fig.6). This can be explained by first considering a conducting layer of uniform re-

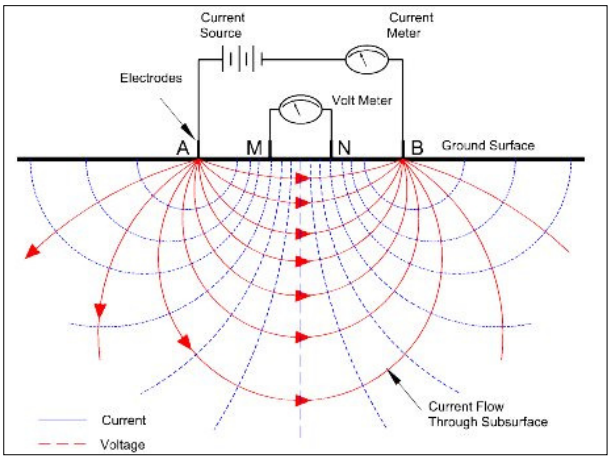

Fig. 6 Resistivity sounding curve (Rowland 2007).

sistivity covered by ground surface and let a current enter at point A (Sharma, 1976). The potential V_P at any point in the ground is then equal to the sum of the voltage from the two electrodes at that point such as

$$V_P = V_A + V_B \qquad (4.5)$$

where V_A and V_B are the potential contributions from the two electrodes A (pos. I) and B (neg. I). By introducing the implication of electrode configuration and its importance it is possible to finally present the relationship between the resistance and the resistivity. When measuring resistivity there are several electrode configurations which can be used. What differ between the configurations are the arrangements of the electrodes. An electrode configuration is characterised by a certain geometry and a resulting geometric factor (K). There is also a close coupling between the geometric factor and the arrangement which describes the relation in distance between the current- and potential electrodes and their mutual distance. The geometric factor takes into account the geometric spread of electrodes and contributes a term that has the unit of length (metres). The geometric factor must be taken in consideration while calculating the resistivity. If the distance AM=NB i.e. Wenner array, then the coefficient K can be calculated as:

$$K = 2\pi\left[\frac{1}{AM} - \frac{1}{MB} - \frac{1}{AN} + \frac{1}{NB}\right]^{-1} \qquad (4.6)$$

where AM, AN and MN are respective distances between electrodes in metres (Reynolds 1997):

$$\rho_a = 2\pi\frac{L^2}{aG}R \qquad (4.7)$$

The apparent resistivity (ρ_a) can be used to further compute the true resistivity of the underground provided that it is completely homogenous (Sharma 1976). In reality the sub-surface does not conform to a homogenous medium and thus the resistivity obtained is not longer the true resistivity but the apparent resistivity (Reynolds 1997). This is further explained in 4.3.

4.1.2 Electrode configurations

The value of the apparent resistivity depends on the geometry of the electrode array used, as defined by the geometric factor K. Only four main types of arrays will be discussed here. A brief presentation of the four arrays is considered to be required to be able to evaluate the suitability of the array applied and the results of the measurements. The different electrode configurations have particular advantages, disadvantages and different sensitivities, which will be explained further.

The greatest limitation of the resistivity sounding method is that it does not take the lateral changes in the resistivity of the layers into account. This will also be explained later.

In the dipole-dipole array (Fig. 7a) both current electrodes are placed together on one side, separated from the potential electrodes on the other. As a result, each side comprises a dipole. The dipoles are separated with a distance na where n is an integer (Jeppsson 2006). The term 'dipole' is misapplied in a strict sense, because by definition the distance between the electrodes of all electrode pairs should be irrelevant with respect to the length of the array. The relevance of this relation makes the term appropriate (Reynolds 1997).

In the Wenner array (Fig. 7b) the current- and potential electrodes are placed with a constant distance, a.

In the Schlumberger array (Fig. 7c) the potential electrodes are placed within a short distance (L) to the measure point which is located in the centre of the array, while the current electrodes are situated at a larger distance.

The Gradient array (Fig. 7d) is an asymmetric version of the Schlumberger array where the measure point, and the potential electrodes, can be placed anywhere between the current electrodes (Jeppsson 2006). This array was used in all the measurements in this work. It has been showed by Dahlin & Zhou (2006) that the gradient array is suitable for multichannel recording and its respective data-acquisition systems. They have also showed that the resolution is better than for the three traditional electrode arrays mentioned. A multichannel system permit recording nu-

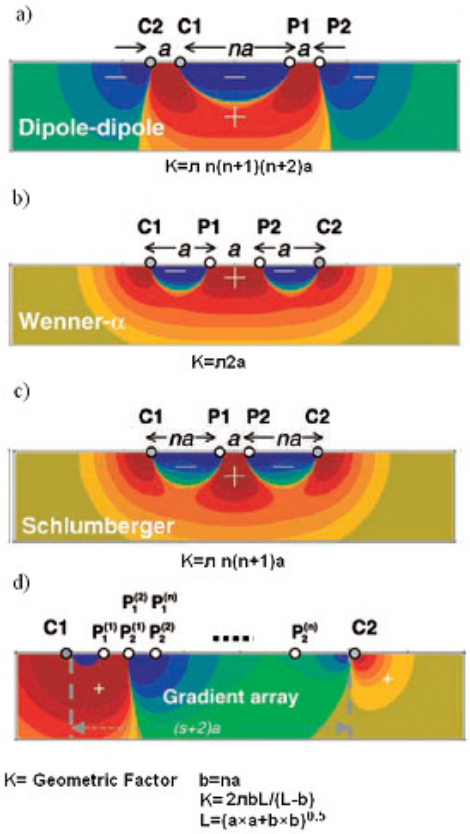

Fig. 7 Electrode configurations and their geometric factors, where **a** is the dipole length, **n** the separation factor. a) Dipol-dipole b) Wenner array c) Schlumberger array and d) Gradient array. The sketch of gradient array showing the position of the electrodes for a measurement with a current-electrode separation of (s+2). Here, the n-factor is defined as the smallest relative spacing between a current electrode and potential electrode (modified from; Dahlin & Zhou 2006).

merous data points simultaneously for each current injection, resulting in significantly reduced fieldwork time without compromising the data density. In a work presented by Dahlin & Zhou (2002) it is showed that the gradient array has a better SNR (Signal-to-Noise-Ratio) than the dipole-dipole method. According to the article the gradient array is elected as a prime choice for multi-channel resistivity imaging both in terms of resolution capability and measurement logistics.

Multi-electrode gradient surveying is carried out by injecting current from the two separate current electrodes and simultaneously or sequentially measuring all the potential differences between the potential electrodes with spacing a. When measuring, a large number of current electrodes are used, scanning across the electrode layout with several different spacing a and/or separations s, see figure 8 (Dahlin & Zhou 2004). Another benefit using the multiple-gradient array is that less different current electrode separations (Fig.8) are needed for a good depth cover in a resistivity imaging survey compared to what is necessary in many others (Dahlin & Zhou 2006).

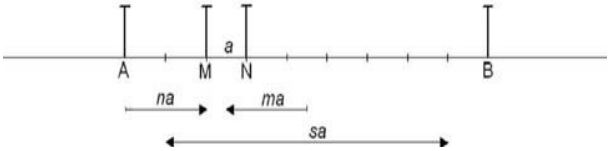

Fig.8 Sketch of gradient array showing the position of the electrodes for a measurement with a current-electrode separation of (s+2) a, where the separation factor s = 7, the n-factor = 2 and the midpoint factor m = –2. Here, the n-factor is defined as the smallest relative spacing between a current electrode and a potential electrode (Dahlin & Zhou 2004).

Here follows some general aspects that should be considered while evaluating an electrode configuration before measuring;

-sensitivity
-SNR (noise)
-required limiting depth
-terrain
-labour intensity

It is important to find out if the array is sensitive to lateral and vertical in-homogeneities and dipping interfaces.

A sensitivity function shows the degree to which a change in resistivity of a section of the subsurface will influence the potential measured by the array (Loke 2003). The structure of the sensitive plots depends on which electrode configuration that is applied. This can be explained by accentuate that the ability to detect a defined volume with a specific resistivity at a certain depth depends on which electrode configuration is used (Loke 2003). Areas with high values in a sensitivity section correspond to the parts that contribute most to the measured resistivity. A prominent reason why the gradient array is applied in this study is that it is sensitive to both horizontally and vertically changes.

During resistivity surveys the voltage is measured. The ground itself gives arise to irrelevant voltages which has to be corrected for. These disturbances are referred to as noise and affect the measured potential difference. The greater the voltage (U) created by the instrument is, in relation to the disturbances generated from the ground (u), the better accuracy in the resistivity measurements. A high SNR-ratio can be obtained by increasing the voltage. A high SNR-ratio can also be achieved by using an array with a low geometric factor e.g. the Wenner array (Jeppsson 2006). Depending on the terrain of the investigation site and its size and labour intensity it may be crucial to consider these parameters.

A large source of field problems can be the electrode contact resistance. This is because the resistivity method relies on being able to apply current into the ground. If the resistance of the current electrodes becomes too high, the applied current may fall to zero and the measurement will fail. High contact resistance is particularly common when the surface material into which the electrodes positioned consists of dry sand, boulders, gravel, frozen ground, ice or laterite. There

are two methods that can be used to overcome high resistance. One is to wet the current electrodes with water or saline solution and the other is to use multiple electrodes (Reynolds 1997).

Equivalence problems imply that structures with different geometry in the ground, displays similar shape in a resistivity section. It is very complicated to make estimations of the vertical distribution of structures found in the resistivity section. This is due to the fact that it is possible to distinguish the top of a structure while the lower boundary is difficult to estimate. It is very important to bear this information in mind during interpretation of resistivity data (Jeppsson 2006).

4.2 Induced Polarization

Induced polarization (IP) is a phenomenon that especially arises in electrically conductive minerals such as sulphides and clay minerals, and was first discovered by Conrad Schlumberger in 1912. The method was developed during the Second World War to detect land mines and its usage has been widely developed since the late 1940s (Reynolds 1997).

IP-measurement can be used as a complement to the resistivity method because of its capacity to differentiate between unweathered and clay-weathered fracture zones. This is important e.g. when evaluating the rock quality at the initiation of a construction work. Low resistivity in fracture zones can depend both on high water- and clay content, while strong IP-effect mainly is due to high clay content.

The measurements are made by using the same type of conventional electrode configurations and equipment as for the resistivity (Reynolds 1997).

When an electrical current is conducted into a body in the ground, the negative (anions) and positive (cations) charges will shift towards the positive respectively negative poles. This process is called electrical polarization and generally occurs in conductive bodies. Some materials have the ability to store these charges after the current has been switched off, and therefore act somewhat like capacitors. This results in a gradual decay of the voltage, called overvoltage decay and can be measured with potential electrodes on the surface. Overvoltage decay is only one aspect of the concept induced polarization which also refers to the initial build-up of the voltage, overvoltage (Reynolds 1997).

4.2.1 Theory

At present the explanations for what causes the IP phenomenon are not clear, but the two models, grain polarization and membrane polarization are commonly used in the literature and serves as a part of the explanation.

Grain polarisation arises in materials that have high electrical conductivity, like metal sulphides, metal oxides and graphite and is therefore of particular interest in surveys for metallic minerals (Loke 2003). When an electrical field is applied over a conductive body it becomes polarized and a reversed electrical field is created which is weaker and orientated in an opposite direction to the main current. At the same time the voltage rises to a level that corresponds to the sum of the applied and the reversed electrical field (Jeppsson 2006). The anions and cations in the body are attracting ions from the surrounding which then attaches to the surface of the body, creating a decrease in the reversed current and an overvoltage (Fig. 9c). When the applied electrical field is switched off, the voltage suddenly drops. The attached ions will then start to diffuse back to the surrounding medium and the polarisation of the grain will reduce in an infinite time which can be measured in terms of decreased voltage.

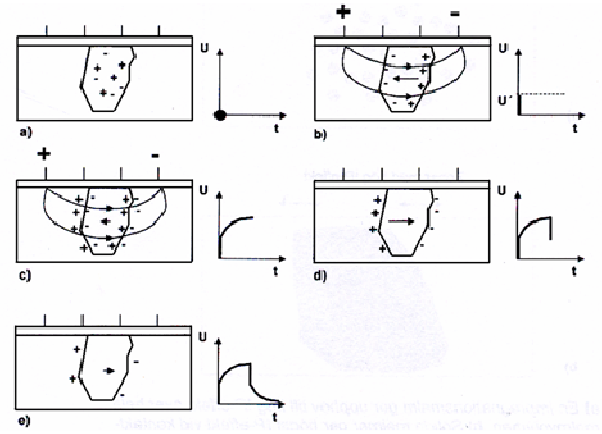

Fig. 9a-c Build-up and decay of the voltage around a grain according to the grain polarisation model (Jeppsson 2006)

Membrane polarization depends on two controls; the size of the pore channels in a material and the presence of clay within pore channels, e.g. in sand (Reynolds 1997). In clay soils the pore diameter is very small and the grain surfaces are negatively charged. This give arise to an attraction between the grains and the positive charges in the electrolyte (water), which produces a positively charged layer around the grain. In places where the layer is thick enough, charged anions will be blocked when an electrical current is induced (Fig. 10a). The relation between the cations and anions creates a potential difference that will gradually disappear when the current is switched off, generating the measured IP.

A presence of clay particles, filaments or fibrous material in the pore channels of a material is another cause for the membrane polarization. Positive ions are attracted to these negatively charged spots, producing a cloud of positive charged ions. This generates a potential difference and thus an IP response when the voltage is turned off (Fig. 10b) (Jeppsson 2006).

4.2.2 Measuring methods

As mentioned earlier, induced polarization is measured in the same way as resistivity. Measurements of IP in time-domain and resistivity can actually be performed simultaneously. During the measurement a known

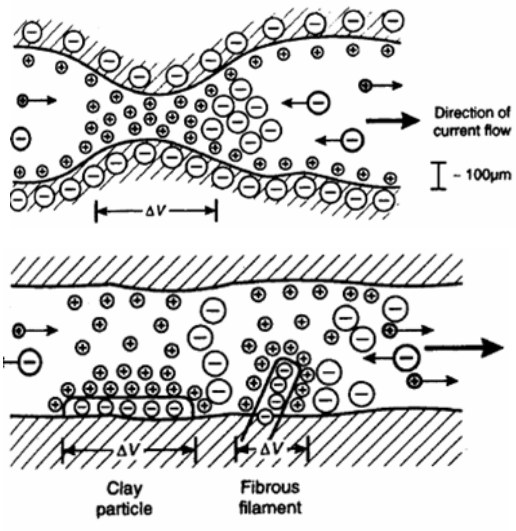

Fig. 10 Membrane polarisation due to a) small poor-channels b) clay particles, filaments or fibrus material in the poor-channel (Reynolds, 1997).

electrical current is applied which creates a voltage that can be measured. The resistivity is dependent on these two variables (Fig. 5) and can therefore be calculated. Resistivity is measured when a current is applied, while the induced polarization is measured after the current has been turned off. Thus when measuring IP, resistivity is automatically obtained (Jeppsson 2006). Compared to the resistivity results, the quality of the IP results is lower because it is more sensitive to different noise sources (Reynolds, 1997).

By measuring IP in time-domain, the variation of the polarisation can be studied during a time-interval. During a measurement the voltage rises as consequence of the applied electrical field. At a certain point the rate starts to decrease until it eventually reaches a constant level (Vo), due to the polarization effects described earlier (Fig. 11). When the field is switched

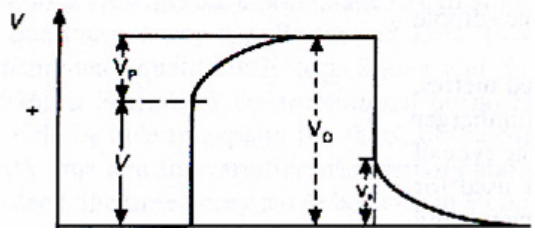

Fig 11 Build-up and decay of the voltage in time-domain measurements (Reynolds 1997).

off, the voltage instantly drops as much as the initial rise and left is the decaying overvoltage. The ratio between polarization voltage (V_p) and the total observed voltage (V_0) is a measure of the IP-effect and is called Chargeability (M) (eq. 4.8) which normally is expressed in millivolt per volt (mV/V).

$$M = \frac{Vp}{Vo} \qquad (4.8)$$

It is very difficult to determine Vp in the instant when the current is shut off because of the fast drop in voltage and therefore the measurement always starts about 10 ms after the shut off. One way to express the chargeability is to describe an area under the overvoltage curve (Fig.12). The area under the curve is an expression of the Vp decay under a certain time period and can be expressed by the following equation;

$$M = \frac{1}{Vo}\int_{t1}^{t2} Vp(t)dt = \frac{A}{Vo} \qquad (4.9)$$

When measuring chargeability the Vp decay can also be divided into several time windows which can provide additional information about the decay, like the character of the decaying curve (Jeppsson 2006).

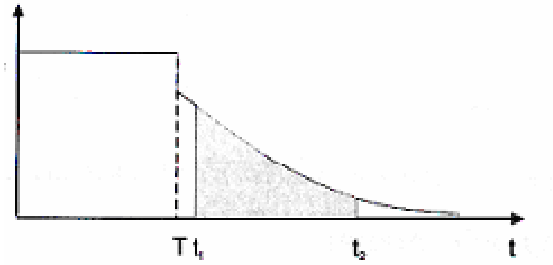

Fig 12 Measurements of chargeability during the overvoltage decay (Jeppsson 2006).

4.2.3 Normalised IP

As mentioned before the IP effect is dependent on both the grain polarisation and the membrane polarization. The normalised IP, defined as the chargeability (M) divided with the resistivity (ρ), quantifies the magnitude of the IP effect that is caused by the grain polarisation (Slater & Lesmes 2002). The normalised chargeability is therefore related to the surface conductivity and can be used to determine if the IP effect is caused by lithology factors or an increased amount of ions. The normalised IP has the unit mS/m.

4.3 Data acquisition and processing of data

The resistivity and IP measurements at the Bolmen tunnel and Ådalsbanan were performed with continuous vertical electrical soundings (CVES). The measurements were based on the LUND imaging system that is designed for optimum versatility in infrastructure projects and environmental studies (ABEM 2007). A measuring procedure consists of the following steps. All four cables are rolled out, and straitened so they together extend to a length of 400 m. Then all electrodes are placed in the ground next to the electrode outlets on the cables. The cables are connected to the electrodes by a jumper i.e. short cable that couples the electrode to the electrode outlet of the cable.

At all times when measuring, the cables are com-

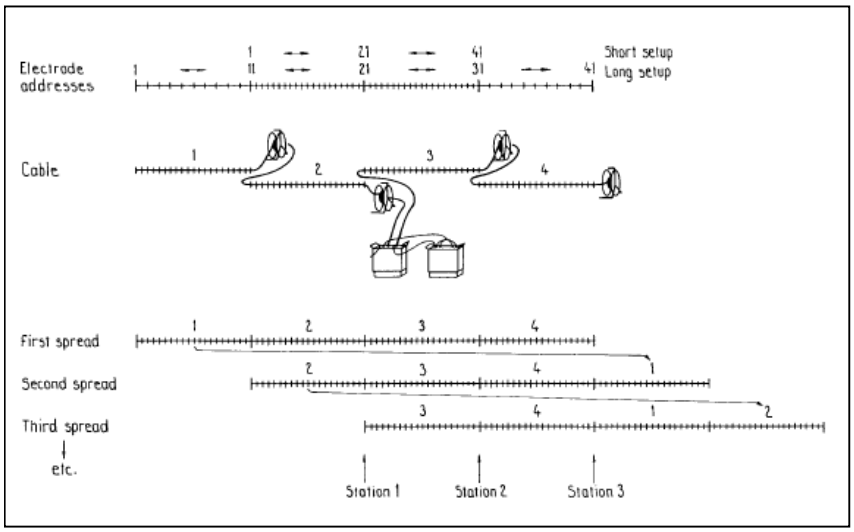

Fig. 13 Schematic sketch of the roll along system (ABEM 2007)

bined with each other, either through a connector or to the instrument. The instrument is first positioned between the first two cables. Before measurement, an electrode contact test is automatically performed to prevent incorrect readings e.g. due to disconnected jumpers or insufficient current. The instrument measures two types of protocols. The long protocol collects data from a large distance by using all cables (usually four) and data from great depths are obtained. The short protocol collects data from a shorter distance and thus from shallower depths, using only the two mid cables.

When the measurements are finished the instrument is successively moved upwards to the position where the second and the third cables are connected. The measurement for a 400 m long profile is completed after moving the instrument upwards, positioned between the third and fourth cable.

A technique called roll along (Fig.13) was used when measuring the 800 m long profiles. After measuring the first four hundred meters the first cable is detached, and rolled up. The first cable is then moved and connected to the end outlet of the last cable.
After moving the instrument forward to the following cables, measurements can be continued. By moving the first cable to the last position the length of the profile increases progressively. The field equipment and instruments used were;

- Four electrode cables (100 m, 21 electrode outlets)
- Steel electrodes
- Electrode jumpers
- Cable connectors
- Portable field computer
- ABEM Electrode selector ES10-64C
- ABEM Booster SAS2000, current transmitter
- Terraohm RIP924 instrument
- Batteries

The instruments that was in used in the field are illustrated in Fig. 14.

Fig. 14 The Instrument case and field computer (photo M. Cegrell).

For resistivity measurements in the field the software used is called Eric software specifically adapted for resistivity measurements. Information on how much current that is injected into the ground is provided. An important benefit with this software is that the entire measuring process can be followed simultaneously in the field via a portable computer, which allows the user to directly control the data quality during measurements.

A 2-D resistivity section is a model of the subsurface where the resistivity is registered in both the horizontal as well in the vertical direction along a profile. This model does not account for the resistivity change that may occur in the perpendicular direction. Therefore it is sometimes necessary to compute a 3-D model in order to get a more complete ground image (Loke 2003). The raw data from a 2-D imagine survey are normally plotted as pseudosections that constitute diagrams that shows apparent (not the real) resistivity values (Loke 1997). However, if the ground is homogenous the apparent resistivity will equal the true resistivity of the ground. In real the sub-surface is often heterogeneous and the measured resistivity value is

then a mean value from different rock lithologies in the ground. The horizontal x-axis in the pseudosection illustrates the measured distance while the vertical axis shows the pseudo (not the real) depth. During evaluation of the measurements, data of poor quality often stand out as extreme points and are readily rejected. In turn, smooth variations of apparent resistivity in a pseudosection indicate data of acceptable quality (Dahlin & Zhou 2006; Jeppsson 2006).

Because the pseudosections only yield a rough estimate of the resistivity on a site, it should not be used as a foundation for the geological interpretation. Before this can be done, the data must be inverted. This process is here performed by a modelling program called Res2Dinv. During this process the program compares the calculated apparent resistivity values with the measured values from the survey in order to reduce the difference between the two (Loke 1997). Every new round with adjustment of the model is called iteration and is normally performed 3-7 times during the inversion to obtain acceptable results. The inversion results give rise to a resistivity model that shows true resistivity values with a real vertical depth axis (Jeppsson 2006).

In this work the robust inversion (l_1-norm) method was used. Compared to the more conventional least square method (l_2-norm) this method emphasizes bodies with sharp boundaries in the ground e.g. igneous dykes or fracture zones (Loke 2003).

A Window based program called Erigraph was used in the final presentations of the sections. Erigraph is primarily designed to facilitate graphical presentations of CVES (2D electrical imaging) data and associated inverted model sections. The measured apparent resistivity can be plotted as pseudosections in colour scale. Inverted sections can be plotted continuous (smooth) or as rectangular blocks. 2D inversion must be carried out using a separate inversion program; in this work Res2Dinv has been used (ABEM 2007).

4.4 Magnetic measurements

Already in the sixth century B.C.E. the Greek philosopher Thales noted the effect of magnetic minerals. The Chinese were however, probably the first to use magnets for navigation. The application of the magnetic method increased during the Second World War and further developments during the 1900th have increased the utility of the method (Nabighian et al. 2005). It is today widely used in various geological disciplines, e.g. mapping of fracture zones and rocks with different magnetic properties and is therefore an important tool in pre-investigations of tunnel constructions (Jeppsson 2006).

In geomagnetic surveys, anomalies in the Earth's magnetic field is studied which can be created by magnetic minerals in the ground. Similar to the planet Earth's geomagnet, a bar magnet has two poles and is surrounded by a magnetic flux which converges near the ends of the magnet, called the magnetic poles. If a bar magnet is subjected to the magnetic field of the Earth, it will align itself with the plus pole pointing towards the North Pole (Reynolds 1997). All material with magnetic properties will, more or less, be magnetized when subjected to an external magnetic field (H_0) meaning that they will create their own magnetic field. This is called induced magnetisation (J_i) and the ability of an object to become magnetized is called susceptibility (k). Material with a high concentration of ferro-and/or ferri magnetic minerals (e.g. magnetite), as basic and ultrabasic rocks therefore has the highest susceptibilities (Reynolds 1997). Another magnetic phenomenon that is common in magnetic rocks or minerals is the remanent magnetisation (J_r). In this case there is measurable magnetic field intensity in the rock although no external magnetic field has been applied. The total magnetic field (H) around a remanent magnetized object is the sum of the external (H_0), the induced (H_i) and the remanent (H_r) fields;

$$H = H_0 + H_i + H_r \qquad (4.10)$$

In geophysical investigations anomalies in Earth's magnetic field (H_0) created by the induced and-/or the remanent magnetisation of magnetic materials is measured. The presence of an anomaly in an investigated area therefore indicates the existence of magnetic bodies in the ground (Jeppsson 2006).

In the investigated sites at the Bolmen tunnel and Ådalsbanan, two different types of gradiometers were used. A gradiometer is a magnetometer that measures the differences in the total magnetic field between two sensors that are placed above each other with a common separation of about 0.5 m. The major advantage compared with a traditional magnetometer is that there is no need of a base-station during the measurements as the two sensors are affected equally. Gradiometer measurements are thus less affected by variations in the earth magnetic field, and the measured anomalies from near-surface objects are more distinct (Reynolds 1997; Jeppsson 2006).

Measurements at Staverhult at the Bolmen tunnel were carried out with a G 858 Magnetic gradiometer, manufactured by Geometrics Ic. Records. At Hallberget and Gårdsberget at Ådalsbanan a GSM-19 Walking Magnetometer, manufactured by GEM System were used.

The data acquisition was performed by measuring back and forth along the same route as for the resistivity profiles. By walking along the same profile at least two times, it enables an estimation of the data quality. The gradiometer used at Staverhult required a steady walking speed to calculate the distance while the gradiometer used at Ådalsbanan had a built-in GPS for this purpose.

4.5 VLF

VLF (Very Low Frequency) measurements were carried out with the purpose to complement the resistivity and IP measurements and, in particular, for detecting

fracture zones. The usage of VLF was limited to a few investigation sites near the Bolmen tunnel, were existing documents indicated a possible occurrences of fracture zones. Only a relatively condensed and simplified presentation of the theory will be follow.

VLF uses radio transmitters within the frequency interval 15-30 kHz. The radio waves are transmitted radially from distal transmitter masts, which originally were used as navigation transmitters for submarines. The waves penetrate the ground and cause induction in materials with good electric conductive capacity. Especially in vertical conductors, induction currents will be generated. The induction gives rise to a secondary magnetic field that is detected with the receiver, a VLF instrument (Jeppsson 2006).

The secondary magnetic field differs from the primary transmitted field in size, phase and geometry. By comparing and studying the difference between the primary- and secondary magnet field, significant anomalies can be registered and used in interpretations of the geology. The secondary magnetic field can be described by two components, in-phase (Re) and out-off-phase (Im) (Jeppsson 2006).

5. Site description and field measurements

The fieldwork was performed in May 2008 and the weather conditions were relatively warm and dry.

5.1 The Bolmen tunnel

5.1.1 Staverhult

The investigation area at Staverhult extending over 900 m, is very flat. The soil cover is relatively deep (4-10 m) and a minor dirt road crosses the site. The area is in a deciduous forest and the ground was wet and covered by thick grass growth. Parts of the investigation site were swamp areas. The topography is mainly following the bedrock surface and the greatest soil depths are generally found in the depressions. Hummocky moraine is dominating, alternating with extensive peat-lands, and scattered glaciofluvial sediments can be found all over. Glaciolacustrine sediments are mainly found in the low-lands. Several different soil types occur in the area which belongs to the southern Swedish uplands. The dominating soil is a sandy-silty till which is relatively homogeneous. In the southwestern area of Staverhult where the resistivity profile was laid out, there is a considerable areal distribution of peat-lands. In the northern part of this area the till is dominating (Olofsson et al. 1988).

There are only a few bedrock outcrops in the Staverhult area. The dominating rock type in Staverhult is a heterogeneous grey-red, often banded gneiss. The banded gneiss is sometime cut by amphibolite dykes, usually 0.1-1 m in width (Stanfors 1987).

In Staverhult (Fig. 15a) one resistivity profile was measured. The profile is 900 metres long with an ori-

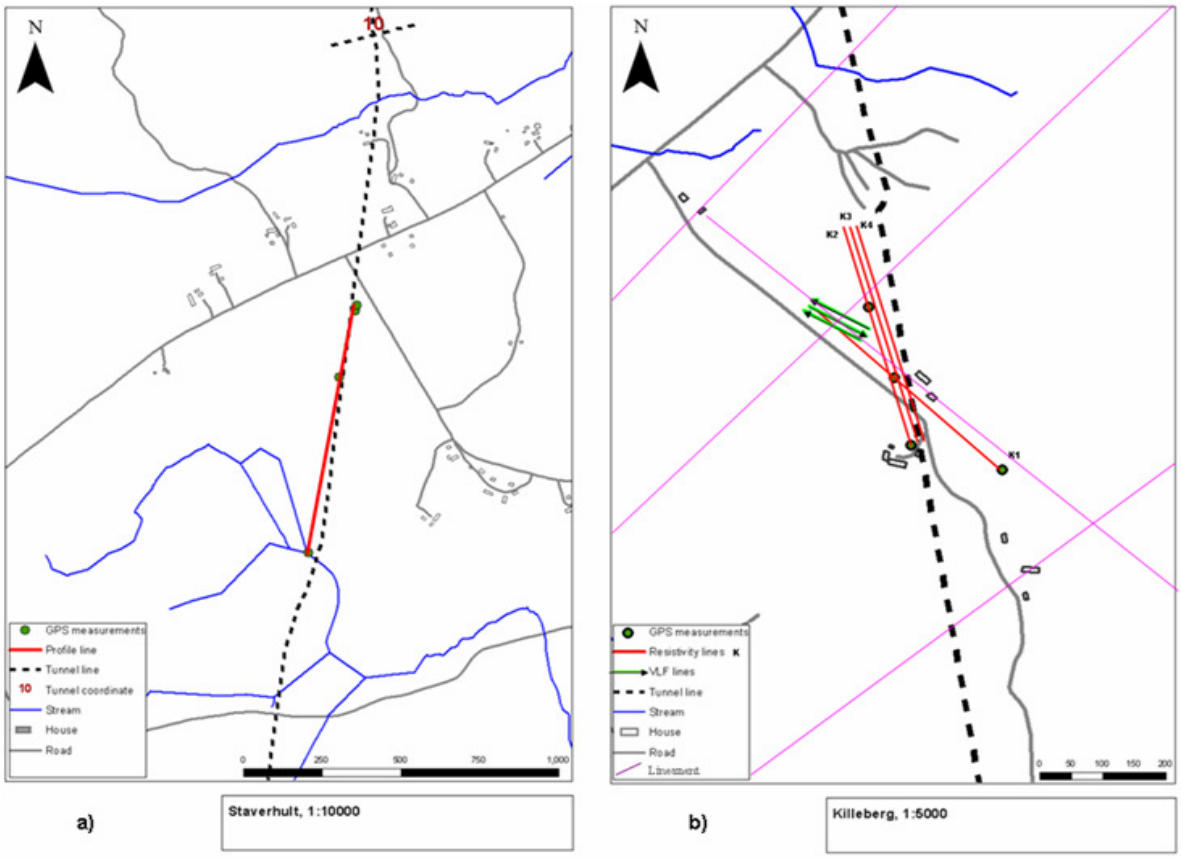

Fig. 15 Map over measured profiles in a) Staverhult b) Killeberg (reworked maps produced by Sydvatten)

entation going from north to south. No electrodes had to be excluded since the electrode contact was relatively good. Along the same resistivity profile, magnetic measurements were performed, going from first north to south and then from south to north. The position of the profile was measured with GPS (Fig.15a). As can be seen, the profile is located right above the tunnel in the first 300 m but then diverges.

5.1.2 Killeberg

Killeberg is situated about ten km north of the first investigated area (at Staverhult) and lies only a few km south of Lake Bolmen where the Bolmen tunnel begins (Fig. 15b). In contrast to Staverhult the landscape in Killeberg is open with meadows and houses surrounded by dense forest. The topography is flat with only small changes in elevation and the soil does not tend to follow undulations in the bedrock surface. The soil depth varies between 1-7 m (Stanfors 1987). The dominating rock type in the area is the common medium-grained, grey-to reddish, gneiss. Dyke swarms of amphibolite often occur and minor weakness zones are present (Stanfors 1987).

At Killeberg, four resistivity profiles with a length of about 400 m were measured. The first profile named Killeberg1 differed from the others because of the orientation going from northwest to southeast. The profile intersects both the tunnel and the other profiles which have a north direction. The other profiles named Killeberg2-4 are parallel to each other and to the tunnel and separated with 10 m. No electrodes were excluded in Killeberg1 because the measurements were carried out in open fields without obstacles and the electrode contact was relatively good along the whole profile. In the last 30 m of the Killeberg2-4 profiles, a large gravel field was encountered which made it difficult to place any electrodes in the ground. Therefore the last six electrodes (30 m) in the profiles were excluded.

Problems occurred during measurements along the Killeberg4 profile why some data points had to be removed. This explains why this profile is shorter than the others. In addition to the resistivity profiles, three VLF profiles were positioned as illustrated in Fig.15b. The position of the profile were oriented perpendicular to one of the lineaments found in the area (Fig 15b). The profiles were 100 m long and were parallel, but with alternated directions. GPS measurements where carried out along the Killeberg1 and Killeberg2 profiles to get a better estimate of the profile position in relation to the Bolmen tunnel.

5.2 Ådalsbanan

5.2.1 Hallberget

Through Hallberget a 750 m long tunnel, from south to north, is planned to be constructed. Hallberget lies along road 90 about ten kilometres north of Kramfors, outside Härnösand. At Hallberget all measurements

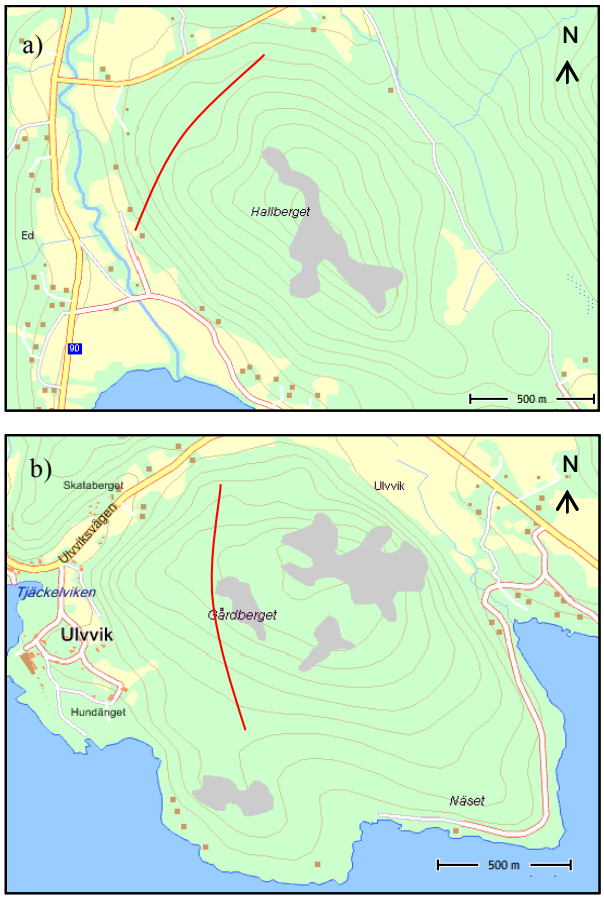

Fig. 16 a) profile at Hallberget (780 m) b) (below) profile at Gårdberget 800 m long (modified from Lantmäteriet 2008)

were performed along a profile that corresponds to the tunnel line (Fig. 16a). In the south, at the tunnel onset, the hill is very steep during the first 200 m with a rise in elevation from about 30 to 90 msl (Fig. 16a).

In general the terrain at Hallberget is made up of forested till and swamp areas (Banverket 2008a). The soil deposits are relatively thin in the northern part along the tunnel line. In most parts of this area the rock is exposed or covered by a thin layer of moss. In the middle and south part of the profile the soil depth is thicker.

The bedrock in the area of Hallberget mainly consists of sediment gneiss (transformed greywacke) which is partially migmatized. In parts along the planned tunnel, granite and pegmatite dykes exist together with longer sections of granite and dolerite dykes. The valleys that are found on both sides of the tunnel coincide with regional fracture zones with a size that varies between 10 to 20 m.

As a whole, the geology in the area is complex, where the southern part of Hallberget is dominated by sediment gneiss and the northern part consists of granite.

5.2.2 Gårdberget

The mount Gårdberget is about 90 msl and extends over 800 m. Topographically, the steepest parts are

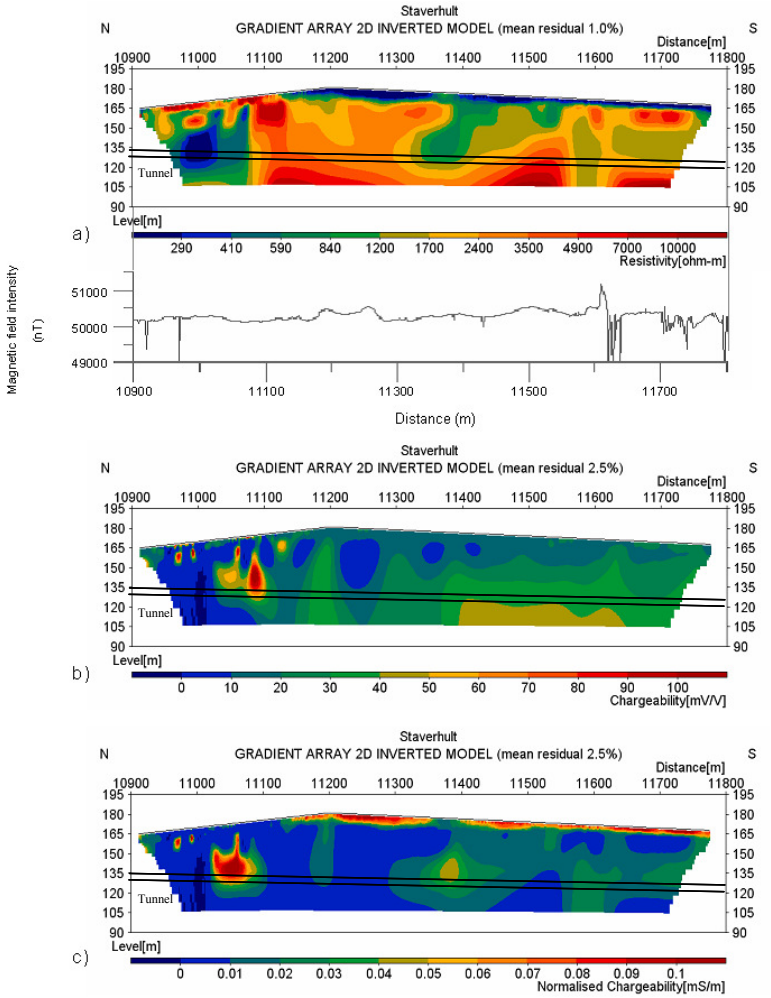

Figure 17 a) Resistivity and magnetic results b) IP results c) normalised IP results for Staverhult

limited to its sides, whereas the middle part at the top is relatively flat. The soil cover was overall poor and sometimes absent, exposing the bedrock. Gårdberget was covered with spruce-, birch- and pine trees growing on thin soil layers that were covered by dry moss.

After the tunnel the railway is planned to run over a valley covered by unconsolidated till and sediments. A great part of the bedrock consists of metagreywacke with subordinate dykes or minor massifs of granite or pegmatite. Other features that exist are loose open joints and fracture zones, whose extent varies. The extent of the fracture zones differs from 10 to 20 m. The investigated area and the measured profiles are presented in Fig.16b and correspond to the tunnel line.

6 Results, Bolmen

6.1 Staverhult

The measured profile in Staverhult lies between the tunnel coordinates 10900 and 11800 m. The electrode separation used in Staverhult was 5 m which using gradient array gave a penetration depth of approximately 60 m. The transmitted current strength conducted into the ground varied between 10 and 200 mA.

6.1.1 Resistivity

The inverted resistivity section for Staverhult is presented in Fig. 17a. The mean residual value is 1.0 % and the total amount of data points is 2872. The resistivity interval in the section ranges between 220-14000 Ωm.

The resistivity variations in the Staverhult section are in general very large, with low resistivity (<290 Ωm) sections alternating with sections of high resistivity (>10000 Ωm). In the interval between x=10900 and x=11120 m the resistivity in the top layer is high and ranges between 4900 and 7000 Ωm. After this section the resistivity becomes much lower and a layer of low resistivity (<290 Ωm) can be followed through the rest of the section. Under the high resistive top layer the resistivity is in general low (220-840 Ωm) with a sharp boundary to higher resistivity values (>1700 Ωm) at x=11080 m. In the top of the low resistive section there are small areas with higher resistivity (1700-7000 Ωm) that alternate with other areas of lower resistivity (290-840 Ωm). Under the top layer between x=11080 and x=11350 m the resistivity is relatively high (1700-10000 Ωm) and consistent. At x=11400 and x=11500 m two zones of relative low resistivity

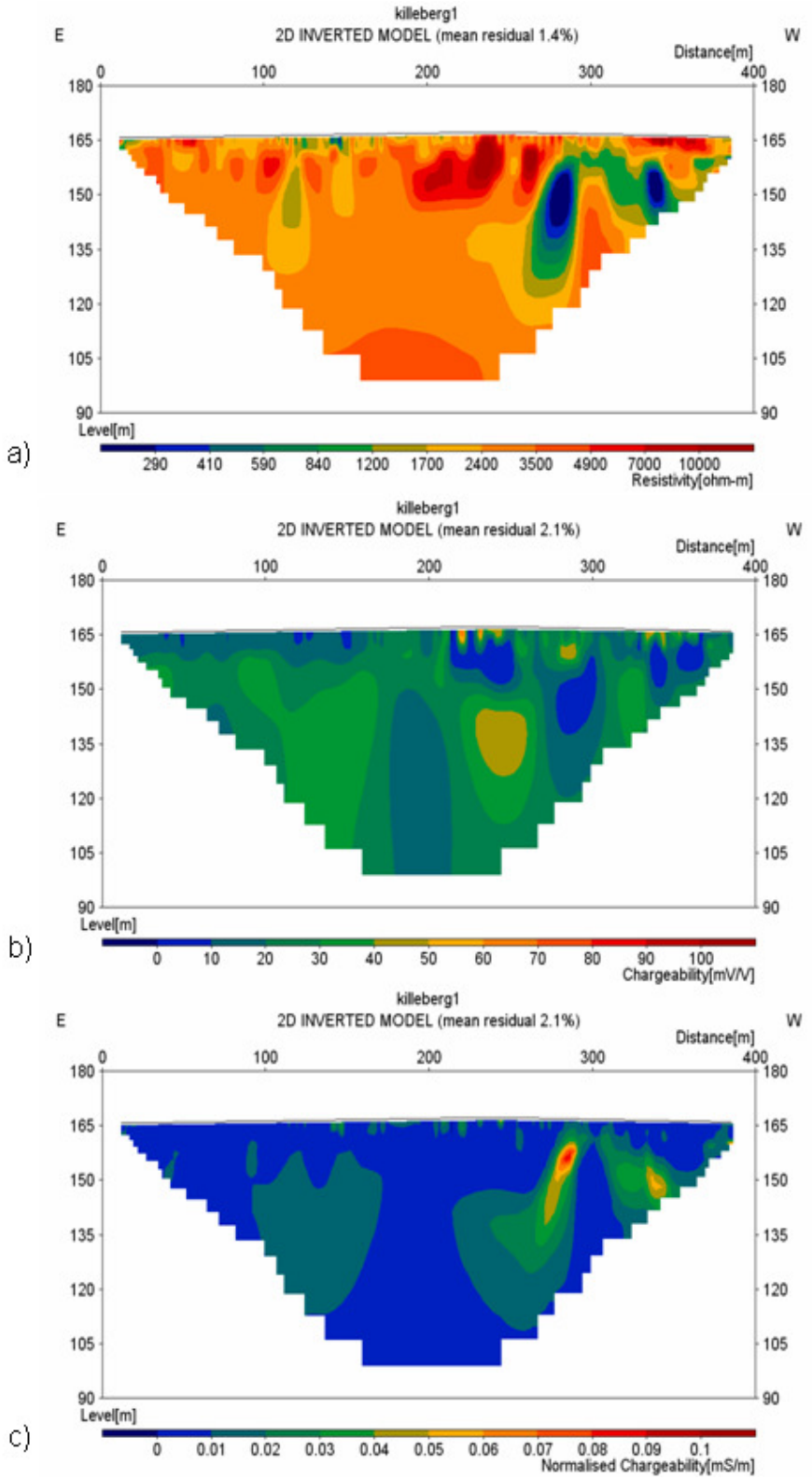

Fig. 18 a) Resistivity b) IP c) normalised IP results for Killberg1

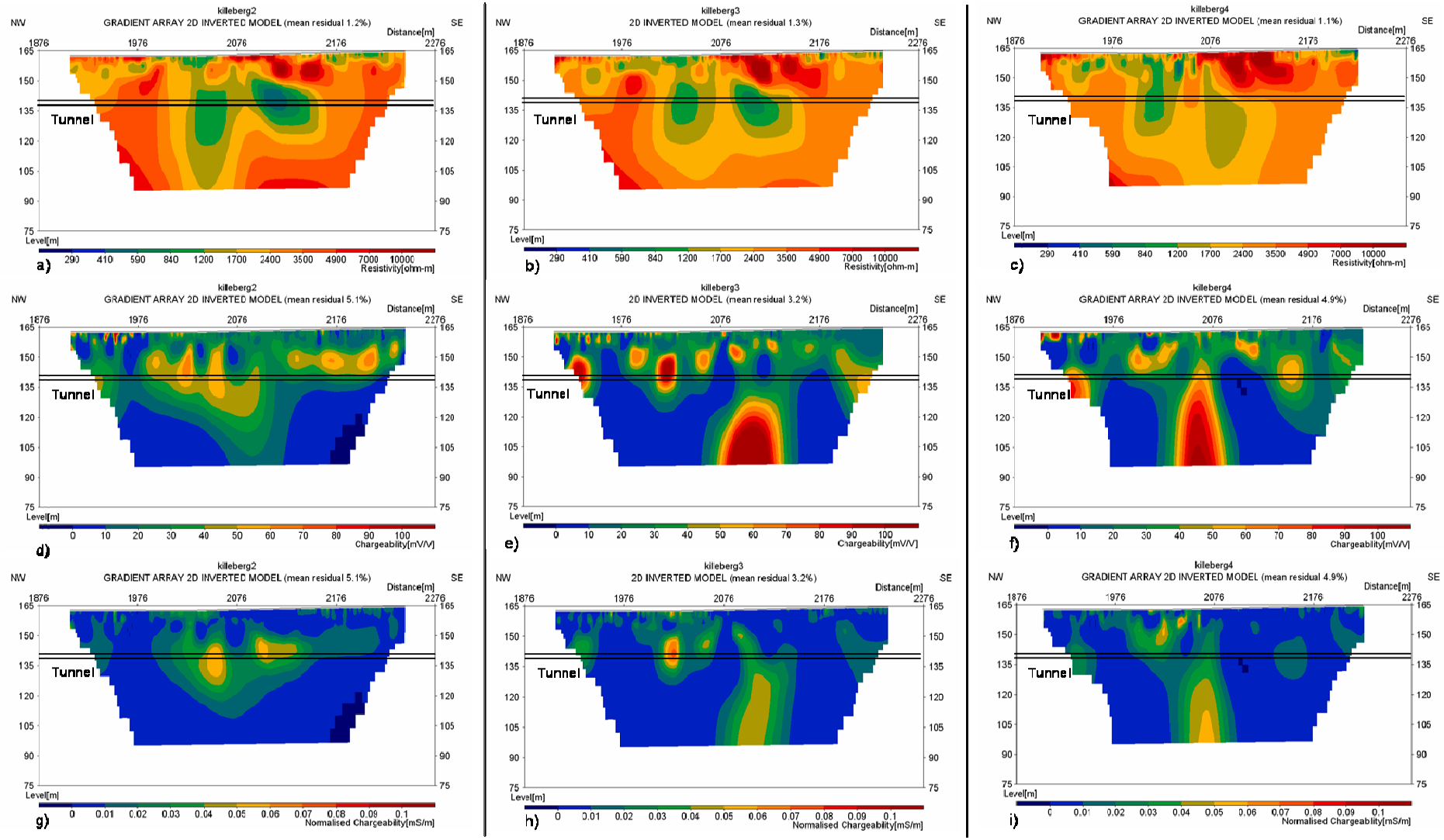

Fig. 19 a-i) Resistivity, IP and normalised IP results for Killeberg2-4

(410-1200 Ωm) are apparent. The first one at x=11400 m is located in a level between approximately 170-130 msl and are approximately 50 m wide. The second one at x=11500 m is smaller and lies shallower at an elevation between 170-150 msl, and has a width of about 40 m. Between these two section the resistivity is slightly higher (1200-1700 Ωm). At x=11600 m a vertical zone of intermediate resistivity (1200-1700 Ωm) is apparent. Between x=11650 and x=11780 m below the low-resistive top layer, a wide horizontal and high resistive (3500-7000 Ωm) zone occurs. Under this zone there is a section of intermediate resistivity (1200-1700 Ωm) and in the bottom the resistivity is high (>10000 Ωm).

6.1.2 IP

The inverted IP and normalised IP sections for Staverhult are presented in Fig. 17b and Fig. 17c respectively. The mean residual value for the IP measurements is 2.5 %. The amount of IP data points is 2872 and the time interval used is 10-30 ms.

The chargeability in the IP section ranges in general between 10 and 40 mV/V, with some smaller areas of higher (40-100 mV/V) respectively lower (<10 mV/V) chargeability. In the top layer along the whole section the chargeability is intermediate (10-20 mV/V). The sections with the highest chargeabilities (40-100 mV/V) are located below the top layer at x=10960 and x=11120 m, between x=11040 and x=11100 m and in the bottom layer between x=11400 and x=11640 m.

High normalised chargeabilities (0.05-0.1 mS/m) can be found at x=10950 m, x=10990 m, between x=11020 and x=11080 m, at x=11380 m, and between x=11120 and x=11770 m in the top layer. Below the top layer at x=11200 m a vertical zone of intermediate (0.01-0.02 mS/m) can be discern because of the low (<10 mS/m) chargeability in the surroundings. The same thing can be seen at x=11600 m.

6.1.3 Magnetic measurements

In figure 17a the magnetometry result is displayed below the resistivity section. In the first 75 m of the profile, two small and very sharp magnetic drops are present. In the following 200 m the magnetic field intensity is relatively consistent. Between x=11175 to x=11275 m there is wide peak in the magnetic diagram which corresponds to an area of high (1700-10000 Ωm) and uniform resistivity in the resistivity section. Here the anomaly reaches approximately 50500 nT before it decreases to 50000 nT again. Between x=11450 and x=11550 m a new, smooth rise of about 500 nT occurs. The most pronounced anomaly in the section occurs at x=11600 m with a sharp rise from approximately 50250 to 51250 nT. Directly after this anomaly there is a drastic drop and irregular shifts in the intensity in an interval of about 20-30 m before it rises to normal values again. The last 100 m of the section is characterised by more irregularities in the intensity. The irregularities were caused by a contact problem in one of the sensor cables and are thus not caused by geological factors.

6.2 Killeberg

The measured profile in Killeberg lies between the tunnel coordinates 1876 and 2276 m. The electrode separation used in Killeberg was 5 m which gave a penetration depth of approximately 60 m. The current transmitted varied between 10 and 100 mA.

6.2.1 Resistivity

The inverted resistivity section for Killeberg1 is presented in Fig. 18a while the inverted resistivity sections for Killeberg2-4 are presented in Fig. 19a-c. The first resistivity section Killeberg1, has 1022 data points and the resistivity ranges between 900-7000 Ωm. Killeberg2 has 903 data points and the resistivity varies between 900-7500 Ωm. Killeberg3 has 841 data points and the resistivity ranges between 900-8700 Ωm. Killeberg4 has 663 data points and the resistivity varies between 800-17000 Ωm. The mean residual value in the resistivity models varies between 1.0 and 1.6 %.

In general, the first 180 m of the Killeberg1 section has a relatively high resistivity (2400-10000 Ωm). Small areas of low resistivity (410-840 Ωm) can be seen at x=120 and x=140 m in the top layer in this interval. The most distinct anomalies in the section are located in the last 220 m. Between x=180 and x=250 m an area of relatively high resistivity (4900-10000 Ωm) is present and is located in a level between approximately 160-150 msl.

About 10 m to the west another narrow high resistivity (4900-10000 Ωm) zone is present lies at the same elevation. At x=280 m between 155-130 msl a vertical zone of low resistivity (290-840 Ωm) is apparent. A similar zone appears in the same elevation at x=340 m. Between these two low-resistive sections the resistivity is higher (2400-4900 Ωm). Above these zones between x=340 and x=360 m, the top layer has high resistivity (4900-7000 Ωm).

In the section for Killeberg2 (Fig 19a), many distinct anomalies are found. The top layer between x=1916 to x=1986 m and x=2066 to x=2116 m shows relatively high resistivity (2400-10000 Ωm), while the top layer in the intervals x=1996 to x=2046 m and x=2166 to x=2226 m seems to have low resistivity (840-1200 Ωm). Between x=2126 and x=2166 m in a level of 160-150 msl another area of high resistivity (4900-10000 Ωm) is present. Under the top layers, between x=2026 and x=2146 m and in an elevation between 150-125 msl, two very large zones with low resistivity (590-1200 Ωm) occurs. At each side of these low resistive zones the resistivity is higher (2400-7000 Ωm).

In the Killeberg3 and 4 resistivity sections the resistivity distribution is in general the same as in Killeberg2 and only minor differences exists.

6.2.2 IP

The inverted IP and normalised IP sections for Killeberg1 is presented in Fig. 18b and 18c while the Kille-

berg2-4 sections are presented in Fig. 19 d-i. The mean residual values vary between 2.1 and 5.1 % in the IP models and the time interval used for the IP is 10-30 ms.

The Killeberg1 is in general dominated by intermediate chargeabilities (20-40 mV/V) throughout the section. However, at x=240 m, x=280 m and x=340 m, areas with higher chargeability (50-60 mV/V) occurs. In the normalised IP section the normalised chargeability is low (0-0.02 mS/m) throughout the section, except at x=280 and x=350 m where it is higher (0.03-0.09 mS/m) than in the surrounding.

In Killeberg2 two extensive areas with relatively high chargeability (50-70 mV/V) occurs between x=1986 to x=2086 m, and x=2140 to x=2230 m, in a level of approximately 160-130 msl. The whole section is in general dominated by intermediate chargeability that varies between 10 and 40 mV/V. Small areas of high chargeability (>80 mV/V) occurs at x=1936 m in the top layer. The highest normalised chargeability (0.04-0.06 mS/m) is concentrated at two round areas at x=2046 and x=2096 m. Around these areas the chargeability is slightly lower (0.03-0.04 mS/m).

At x=1926 m, x=2026 m and x=2116 m in Killeberg3 the chargeability is very high, up to 100 mV/V. Other areas with slightly lower chargeability (50-70 mV/V) also occur along the section. In the normalised IP section a vertical zone of high normalised chargeability (0.05-0.06 mS/m) is apparent at x=2100 m. High normalised chargeability also occur at x=2016 m. In general, the same chargeability and normalised chargeability distribution can be seen in the Killeberg4 section.

6.2.3 Resistivity, 3-D

In fig. 20 the results from 3-D resistivity inversion are illustrated. The inversion was made for the three parallel profiles Killeberg2-4 and four slices from shallow depths are presented. In the first slice at 1.9 m depth, two sections of high resistivity (4900-10000 Ωm) occurs at x=1876 to x=1900 m, and x= 2076 to x=2126 m. Areas of low resistivity (840-1200 Ωm) are present at x=1976 to x=2026 m, and x=2160 to x=2230 m. In the rest of the section the resistivity is moderate (1700-2400 Ωm). Further down, at 3.5 m depth the resistivity distribution is in general the same as in the first slice. At 5.3 m depth the high resistive area at x=1876 to x=1900 m has been reduced while the other high resistive area is more pronounced. The distribution of the low resistive areas has decreased and are absent in the southern part of the section. In the last slice at 7.3 m depth the high resistive area in the northern part has disappeared and the most of the low resistive areas are gone.

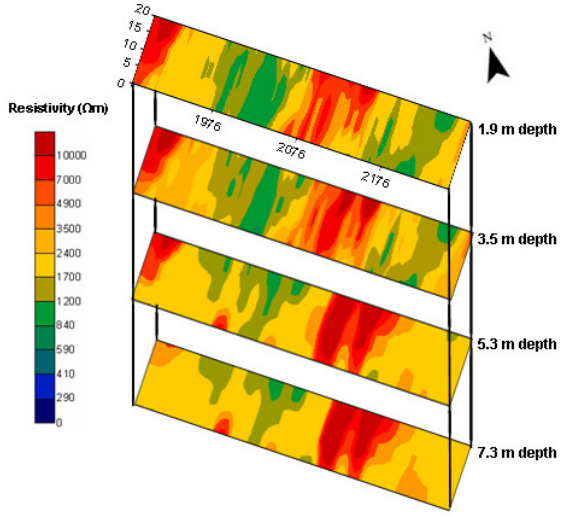

Fig. 20 Results, 3-D Resistivity

6.2.4 VLF

The VLF results are displayed in Fig 21. In the first profile (VLF 1), the relationship between the in-phase (Re) and out-phase (Im) curves most likely illustrates an anomaly between x=0 and x=65 m. In the first 40 m the in-phase curve rises and then decreases, and has greater values than the out-phase curve. After x=40 m there is a shift, and the out-phase curve gets higher values than the in-phase curve. After this the out-phase curve decreases and the in-phase curve is constant.

The second VLF profile appears differently than the first profile. From the beginning the values constantly decreases and the out-phase curve lies above the in-phase curve, throughout the section.

The third VLF profile is similar to the first, but has greater values in the beginning. Between x=0 and x=65 m the in-phase curve is larger than the out-phase

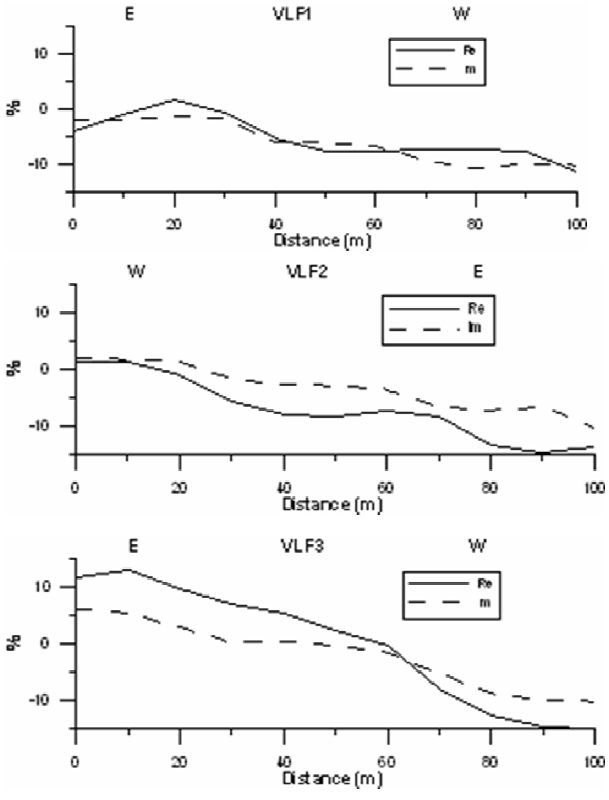

Fig. 21 Results from the VLF measurements: VLF 1 (top), VLF 2 (centre) and VLF 3 (below) at Killeberg.

curve. After x=65 m, the in-phase curve lies above the out-phase curve.

7. Discussion, Bolmen

As mentioned earlier in this work, a research project including scientist from different departments of technical universities in Sweden where founded in 1983. The project was concentrated to a small part of the tunnel near the Staverhult village. The amount of reference data from this area is significant compared to the other investigated sites at Killeberg. Further, the data quality and resolution for the IP and resistivity sections are regarded as high because of the low mean residual values obtained during the inversions.

7.1 Staverhult

In Fig. 22 the resistivity section for Staverhult has been divided into different zones that are interpreted to be of geotechnical importance for the Bolmen tunnel.

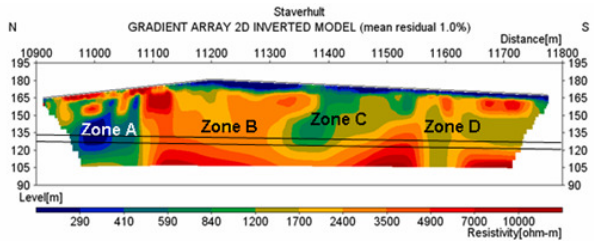

Fig. 22 Zones of varying properties in connection to the Bolmen tunnel in the Staverhult resistivity section.

Zone A in Fig. 22 is characterized by low resistivities (200-500 Ωm), which indicates that this part of the bedrock is of relatively low quality, more fractured than the surrounding rock. The Bolmen tunnel cuts through this presumably fractured section in a depth of approximately 30 m below the ground, between the tunnel-coordinates 10900 and 11080 m (see Fig. 22). In the centre of **Zone A** low chargeability (<10 mV/V) is apparent which indicates that the fracture zone is filled with water. In the margin of the zone at x=11080 m a sharp contact between low and high resistivity (1700-10000 Ωm) is prominent and characterised by high chargeability that probably indicates clay weathering in the contact. In the top of **Zone A**, small parts with higher resistivity alternate with small parts of low resistivity. Some of the low resistive areas also have high chargeability which again indicates local clay weathering or mineralization. The top of **Zone A** most likely shows the upper surface of the bedrock as a sharp boundary to the high resistivity that characterizes the layer above. The high resistive top layer corresponds to sandy till. In the first 50 m in the magnetic diagram two small and sharp drops in the magnetic field intensity can bee seen. These two drops are belived to reflect contact problem during the measurements.

In **Zone B** the resistivity is consistently higher compared to in **Zone A,** and varies between 1700 and 10000 Ωm. In this section the bedrock is less fractured. The chargeability and the normalised chargeability in the zone is relatively low (<40 mV/V and 0-0.04 mS/m) while a wide peak in the magnetic diagram is apparent. The magnetic peak corresponds to increased magnetic properties in the gneiss bedrock which most likely are caused by amphibolite swarms or dykes. The only rock types along the tunnel route that would be expected to give magnetic anomalies, except amphibolites, are basalt and dolerite dykes. Basalts and dolerite dykes are however expected to be located in the southern part of the tunnel and not in the investigated areas (Stanfors 1987). In the top layer above **Zone B** the resistivity is low (<290 Ωm) throughout the section. The chargeability is moderate (10-20 mV/V) whereas the normalised chargeability is high (0.05-0.1 mS/m). This section coincides with the moist peat areas that were crossed during the measurements.

Zone C is characterised by low resistivity, a zone that is also cut by the Bolmen tunnel. This zone is interpreted as dominated by crushed and fractured rock with high water content. The relatively high chargeability (50-60 mV/V) and normalised chargeability (0.05-0.06 mS/m) in the bottom of the zone indicates clay weathering or secondary mineralization. Further south, at x=11500 m a smaller zone of low resistivity can be seen which corresponds to a smooth rise in the magnetic field intensity. The magnetic peak probably corresponds to an area where amphibolites are more frequent, while the low resistivity corresponds to a fractured section in the upper part of the bedrock.

Zone D is characterised by a sharp peak in the magnetic field intensity of about 1000 nT that is coincident with a vertical zone of intermediate resistivity (1200-1700 Ωm). This indicates the presence of an amphibolite dyke or a dense concentration of smaller amphibolite bodies. In the last 140 m in the resistivity section, below the low-resistive top layer, a horizontal high-resistive zone overlays a zone of lower resistivity which probably reflects higher respectively lower quality of the bedrock. The irregularities in the magnetic diagram in this interval are due to the contact problem.

The interpretation based on IP and resistivity measurements is in excellent agreement with the results of the tunnel mapping made during the excavation of the tunnel in Staverhult (see appendix B1). **Zone A** correlates to a section between x=10900-11000 m dominated by crushed rock and significant clay weathering. Between x=10300-10400 m a large amount of amphibolites has been documented which coincidence with the magnetic peak observed in **Zone B** and **C** (between x=10290-10360 m). Furthermore, a fractured and crushed section between x=10380 and x=10420 m coincidences with the section the tunnel cuts **Zone C**. The magnetic peak in **Zone C** at x=10500 (Fig. 22) is supported by the presence of amphibolites observed during the tunnel mapping. Amphibolites have also been documented at x=10600 m which coincidence

with the magnetic peak in **Zone D**.

7.2 Killeberg

In Fig. 23 and Fig. 24 the resistivity sections for Killeberg1 and 2 has been divided into different zones that are interpreted to be of geotechnical importance for the Bolmen tunnel. Killeberg2 is representative for all the parallel profiles (Killeberg2-4) since they all display the similar resistivity patterns.

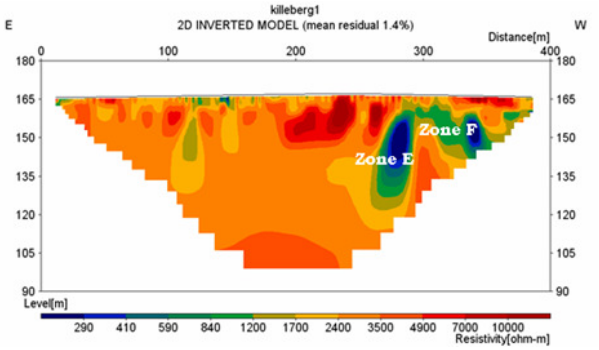

Fig. 23 Zones of varying properties in connection to the Bolmen tunnel in the Killeberg1 resistivity section.

Zone E and **F** (Fig. 23) in the Killeberg1 resistivity section are both characterised by low resistivities (<290 Ωm) which implies that these sections constitute fractured and water-rich bedrock. Relatively high chargeability (50-60 mV/V) together with high normalised chargeability (0.06-0.1 mS/m) in the top of **Zone E** shows that clay weathering or mineralization may be significant. The occurrence of fractured rock in this part of the sections is supported by the occurrence of a lineament that crosses the resistivity profile in this interval (see Fig 15b). Between the low-resistive zones the gneiss has higher resistivity (2400-4900 Ωm) and should thus be of higher quality.

Further to the East a wide section of high resistivity (>4900 Ωm) is prominent. This section can also be seen in all the parallel profiles in the interval were they intersect Killeberg1. The high resistivity suggests that this part of the bedrock is less fractured and more solid compared to the surrounding rock. High resistivities (>4900 Ωm) in the top layer could correspond to sandy deposits, e.g. sandy till or glaciofluvial sediments. However, since the resistivity is very high it is more likely that these sections correspond to areas where the bedrock lies shallower with only a thin soil cover. Low resistivity in combination with low chargeability in the top layer most likely corresponds to soils with high water content. At approximately x=2100 m the chargeability is high in the top layer which indicates a high clay content.

In **Zone H** and **I** (Fig. 24) two large and pronounced areas with low resistivity (410-1200 Ωm) and high chargeability (40-60 mV/V) occur in all the parallel sections, which indicates the presence of clay weathered fracture zones. The IP effect could also be due to mineralization in the zones. As can be seen in the resistivity sections the Bolmen tunnel cuts through these sections. The two zones also coincide with the areas in which two lineaments cross the profiles (Fig. 15b). The first one is going in E-W direction whereas the second is the same SW-NE trending lineament that crosses the end of the Killeberg1 profile. **Zone F** in Killeberg1 and **Zone H** in the parallel profiles can therefore be connected to one common SW-NE going fracture zone. At each side of **Zone H** and **I**, the resistivity is higher and the rock quality better (**Zone G** and

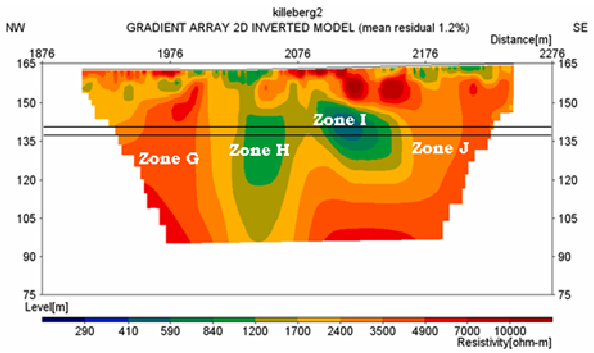

Fig. 24 Zones of varying properties in connection to the Bolmen tunnel in the Killeberg2 resistivity section.

J, Fig 24). **Zone I** in the parallel profiles can probably be connected to an E-W going lineament which also is interpreted as a clay weathered fracture zone.

Data from the tunnel mapping in Killeberg is presented in appendix B2. Fractured and crushed zones has been documented between x=1980 and x=2100 m which can be correlated to **Zone H** and **I** in the resistivity section (Fig. 24).

The resistivity sections here presented can also be used to make a relatively rough estimate of the depth to the bedrock. In general, the resistivity of solid gneiss would be expected to have higher resistivity values compared to the e.g. a wet sandy soil. The contrast in resistivity can therefore be used to distinguish between the two lithologies. As can be seen in the interpretation of Killeberg2 (Fig. 25), the soil thickness varies greatly along the section, approximately between 1 and 7 m. In the two areas in the top layers where the resistivity is low (840-2400 Ωm), the soil depth has been interpreted to be greater than in the areas where high resistivity (>4900 Ωm) is apparent.

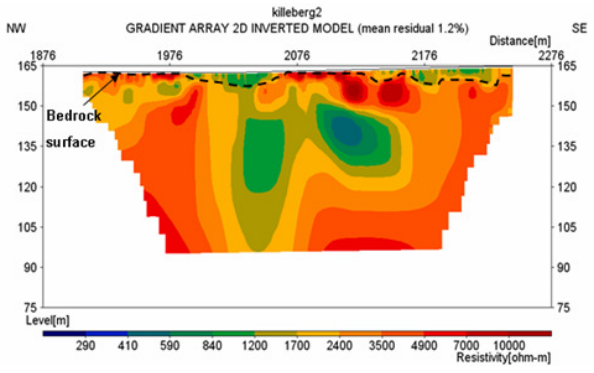

Fig. 25 Estimated depth to the bedrock in the Killeberg2 resistivity profile.

To obtain a more exact estimate of the depth to the bedrock a 3-D inversion was made for the three parallel profiles (Fig. 20). This enables a better overview of the resistivity distribution between the profiles and serves as a complement to the interpretation. The 3-D slices presented in the results show the same resistivity distribution as the top layers in the 2-D section, as expected. The low resistive layers gradually decrease downwards and generally disappear at 7.3 m depth. This confirms the estimated maximum depth that was interpreted from the 2-D section. In summary, the bedrock lies shallow between the tunnel coordinates x=1876-1976 and x=2076-2176 m while greater depths (up to 7 m) are located at x=1975-2045 m and x=2125-2230 m. A better resolution in the resistivity section could be achieved by using a smaller electrode spacing (e.g. 2.5 m). This however, would have provided a less penetration depth which was not desirable in this work.

Additional to the resistivity and IP measurements, a small VLF survey was performed. The VLF profiles were placed out west to the resistivity profiles and in another direction (Fig. 15b). The reason for this was to establish the existence of the fracture zone that had been indicated by the lineament earlier mentioned. The results show that anomalies are apparent in the first and the third VLF profile (Fig 26). These anomalies correspond well to the location of lineaments crossing the profiles. Measurements along the second profile seem to have been disturbed that may be due to a temporary weak VLF signal.

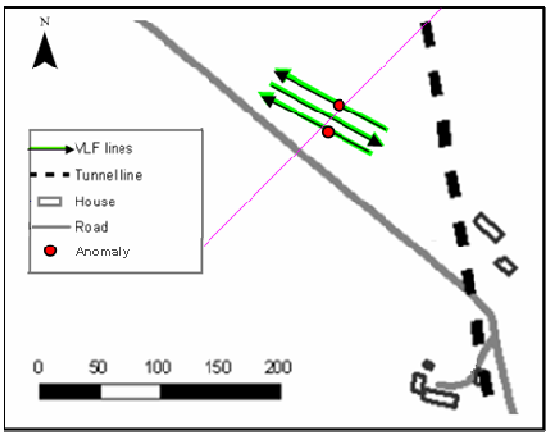

Fig. 26 The location of the VLF anomalies along the measured profiles

8 Results, Ådalsbanan

8.1 Hallberget

At Hallberget all measurements were performed along a profile that corresponds to the tunnel line. All sections are presented from south to north and include the topography. The mount Hallberget reaches a height of about 90 msl and is 30 msl at its foot. The southernmost 200 m is rather steep whereas the rest of the topography only varies between approximately 5 and 10 m vertically. The profile at Hallberget has the railway coordinates x=473200 to x=474000 m (with Stockholm as a reference point). Consequently, the length of the profile is 800 m.

During the resistivity measurements at Ådalsbanan poor electrode contact was occasionally noted. This problem was to some extent expected as dry moss directly overlies the bedrock in many places. By using water and/or multiple electrodes this problem could often be overcome. All measuring results from Hallberget are presented in Fig.27.

8.1.1 Resistivity

The inverted resistivity section is presented in Fig. 27a. The depth of penetration was approximately 75 m. The mean residual for the inverted resistivity is 5.4 % and the resistivity values are between 50 and 27500 Ωm. The minimum respective maximum current transmitted was 10-100 mA. The number of datum points was 2369.

The resistivity at the southernmost part of the profile varies both vertically and horizontally. Low resistivity values (<290 Ωm) exist at the beginning of the profile between x=473200 and x=473230 m, but is abruptly followed by a high resistive (>7000 Ωm) region x=473230 to x=473300 m. During the next hundred metres several changes occurs which can be observed in the section. First of all, a high resistive (>7000 Ωm) zone is found at x=473300 m that continues to approximately x=473340 m, thereafter the resistivity more or less gradually decreases. The following section at x=473350 to x=473450 m is characterised by relatively low resistivities (<2400 Ωm). This section is covered by a thin layer of low resistivity. At x=473450 to x=473600 m a significant low resistive layer (<1200 Ωm) at a depth of approximately 10 m exist, which is covered by a more high resistive layer. Each of these layers has a vertical extent of about 15 m.

Another abrupt shift occurs from low to high resistivity at x=473600 m. Until x=473680 m the resistivity in this part is almost completely homogenous, both vertically and horizontally downwards to the end of the profile. This rock volume is situated under a topographic low, and the surface is a swamp area. Note the low resistive topmost layer (<290 Ωm) within this part. After x=473780 m there is a rise in the topography, and a low resistive (<290 Ωm) body is present only a few metres under the subsurface. The resistivity gradually decreases outwards from its centre. There is a substantially difference in resistivity between this object and the surrounding rock. The last part x=473820 to x=473980 m is considered to be almost homogenous and is characterised by high resistivities.

8.1.2 IP

The inverted IP section for Hallberget can be seen in Fig. 27b. The time interval used for the IP is 10-30 ms. The mean residual value for the inverted IP section was 8.1%.

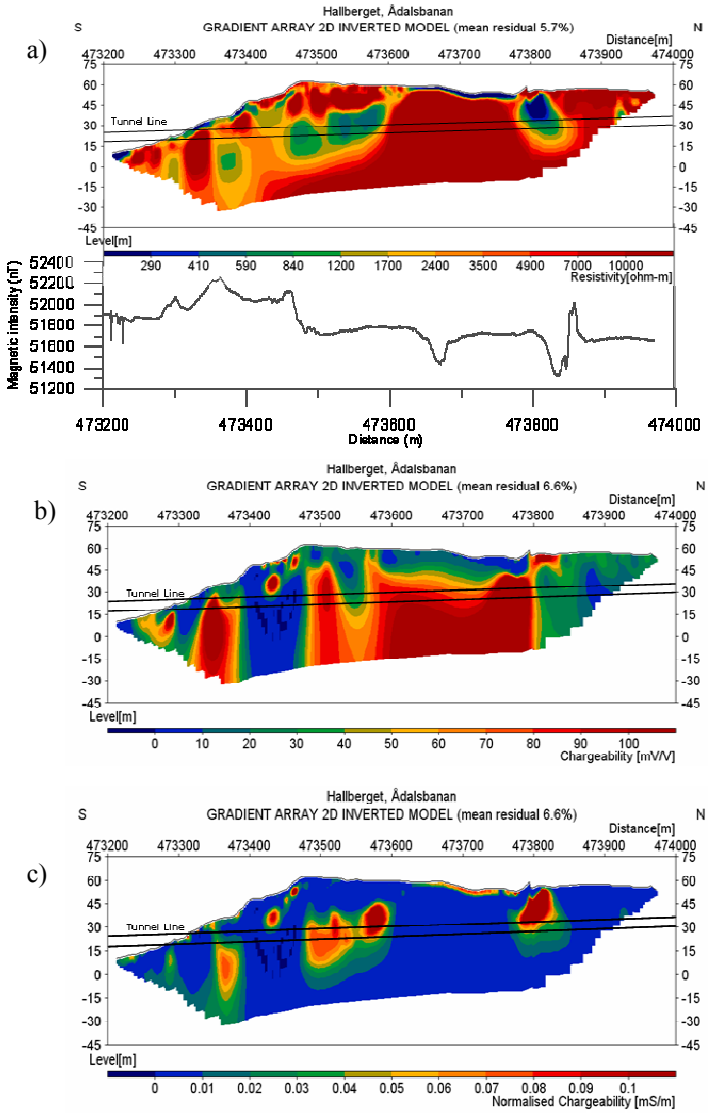

Fig. 27 a) Inverted resistivity and a magnetic diagram b) IP section, c) Inverted IP section, Hallberget

Four distinct anomalies appear in the section. First, after an increase in the topography at x=473290 m a limited section with high chargeability appear. At x=473350 m a large section with high chargeability (>100mV/V) is found at a depth of 2-3 m. The chargeability gradually decreases downwards to the end of the IP-section.

After a region of low chargeability a sudden shift occurs at x=473470 m. Here, the chargeability starts to increase (>50mV/V). However, this change is restricted to layers found at great depth. The significant rise in chargeability continues but drops again, and the upper part within the distance x=473520 and x=473560 m is characterised by low chargeability. This decrease in chargeability is then followed by a steady increase at x=473560 m. The following 300 m i.e. x=473490 to x=473830 m involves two regions showing high IP-effect (>90mV/V). One is found at x=473570 m at a depth of 15 m and the other at x=473840 m at a depth of about 8 m. Even after this distance high chargeability continues until x=473840 m, but is now restricted to the uppermost layer.

Fig. 27c shows inverted normalised IP, and thus showing how the chargeability changes independently of the resistivity. In the section four distinct anomalies appears, showing normalised IP-effect (>0.1mS/m). The first is found at x=473340 m at a depth of approximately 8-10 m. A second anomaly is situated at x=473480 m and a third appears almost right after. The last two are both found at a depth of ca 20 m. The fourth anomaly is situated at x=473780 and extends to x=473820 m.

8.1.3 Magnetic measurements

The magnetic diagram is displayed below the resistivity section (Fig. 27a). It shows many positive and negative anomalies. This facilitates the possibility to study and compare the diagrams. In the first part until x=473250 m a few narrow, but great dips can be observed. Thereafter at x=473400 m, two positive anomalies are apparent and followed by a gradual decrease in magnetic field intensity until x=473460 m is

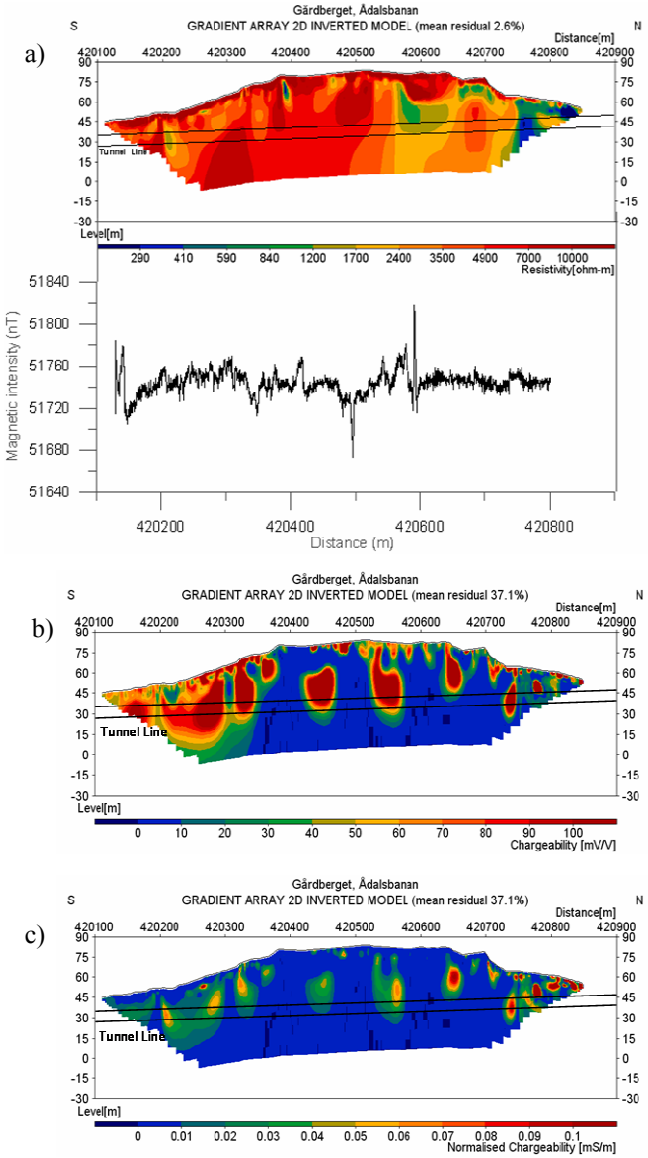

Fig. 28 a) Inverted resistivity section and a magnetic diagram b) Inverted IP section and c) Inverted normalised IP section, Gårdberget.

reached, where a rapid shift toward increasing intensity occur. After this small positive anomaly, there is an apparent drop, and the magnetic field intensity goes from 53000 nT down to 51800 nT. This drop occurs within only a few metres. After x=473760 m another strong negative drop (almost 51400 nT) that immediately rises to about the same level as earlier. A distinct change occurs at x=473920 m, first by dropping to an extreme value of 51300 nT which then rises to 52000 nT.

8.2 Gårdberget

All measuring results from Gårdberget are presented in Fig. 28.

8.2.1 Resistivity

The resistivity values range between 160 and 23000 Ωm. The mean residual for the inverted resistivity is 2.6%. The transmitted current at Gårdberget was in the range 5-20 mA, which is very low. The number of datum points was 1900.

The inverted resistivity section (Fig. 28a) is characterised by high resistivity values, although some exceptions prevail. The first two thirds of the section (x=420100 to x=420550 m) are made up mainly by high resistivities, where only small variations occur. However, at x=420380 m a relatively shallow point source with significantly low resistivity (<1200 Ωm) appears. At x=420550 m the resistivity starts to decrease, and a restricted low resistive region (<1200 Ω m) can be observed at x=420560 m at 5-20 m depth. The resistivity thereafter gradually increases downwards. There is no change in the resistivity at the surface above this section. At depth, low resistivity continues, while the uppermost is characterised by high (>7000 Ωm) resistivities. The last part from x=420750 to x=420870 m characterises a low resistive region. In the last part x=420800 to x=420900 m the resistivities are almost constant below 1200 Ωm.

8.2.2 IP

The inverted IP section from Gårdberget is presented in Fig. 28b. The time interval used at the measurements was 10-30 ms.

Several apparent anomalies can be observed in the inverted IP section. Within the distance of x=420250 and x=420360 m, three regions with high chargeability are present close to the surface. Another anomaly is found at x=420450 m at a depth of 20 m which displays a sphere shaped symmetry. Two prominent anomalies, both near the surface are located at x=420530 and x=420620 m. The potential chargeability of these anomalies exceeds 100mV/V.

The inverted normalised IP section is presented in Fig. 28c. About six minor anomalies can be seen in this section. Most of them has a restricted distribution and are located at about 15 m below the surface. The normalised chargeability (0.1mS/m) decreases outwards from their centres. The first two are located at the distance x=420280 to x=420300 m and can be observed in the section (Fig. 28c). The third is found at x=420460 m and has lower chargeability than the previous two. The fourth- and fifth anomalies are located at x=420650 and x=420750 m. The last part x=420750 to x=420870 m is a region where the normalised chargeability alternate frequently (0.01-0.1mS/m).

8.2.3 Magnetic measurements

The magnetic field profile for Gårdberget is displayed below the resistivity section (Fig. 28a). The magnetic measurements extended for 670 m. The diagram reveals only a moderate variation in magnetic field intensity, although a few significant drops and peaks exist.

After only a few metres a sudden increase occurs that is followed by an immediate drop (51760 - 51710 nT). Thereafter minor variations occur until x=420300 m when another rapid increase takes place. At x=420460 m an even larger drop (<51680 nT) exist. Then an immediate rise of the magnetic field intensity occurs. After a gradually increase a maximum peak is reached (51820 nT) at x=420560 m. Thereafter no significant change in the magnetic field intensity can be observed.

9 Discussion, Ådalsbanan

All conclusions and assessments are based on the results that so far have been presented in this study.

9.1 Hallberget

There are several zones found at Hallberget that are thought to have technically significance. In Fig. 29 a rough division of the zones (A-G) are presented, which are considered to be important during the construction of the tunnel from a technical perspective.

During the first 50 m (x=473200 to x=473250 m) of Hallberget the resistivity is highly irregular. The cause of these variations is probably linked to fractures (low resistive) and occurrence of pegmatite dykes of more resistive character. It is most likely that clay weathering appears in association with some fractures, since the chargeability is high. This sequence probably comprises of rock with poor quality and the stability is most certainly low.

Zone A (x=473280 to x=473320 m) is characterized by relatively low resistivity and chargeability (Fig. 29). At about the same distance in the magnetic diagram a shift from high to low magnetic field intensity occurs. This zone is interpreted as a weak zone situated right next to a dyke. Weathering and precipitation of secondary minerals in fractures might be expected. Zone A is thus regarded as a fracture zone with poor stability and quality.

Zone B (x=473320 to x=473350 m) is a high resistive region (Fig. 29). According to the IP- and the normalised IP the zone is characterised by low chargeability. The magnetic diagram reveals a significant peak that appears to correlate with this zone. Zone B is interpreted as a mafic dyke. This is supported by the fact that mafic dykes typically show high resistivity and low chargeability. In addition, the presence of a mafic dyke usually results in an enhancement of the magnetic field intensity. Further support is the indication of fracture zones (A and C) that surrounds Zone B. Lithological contacts often represent natural zones of weakness, along which deformation is localised upon stress. The stability of Zone B depends on grain size, pore content and presence of weathering.

Zone C (x=473350 to x=473400 m) is a low resistive region with high chargeability (Fig. 29). In the magnetic profile a decrease of the intensity occurs. This zone is identified as another fracture zone of similar character as Zone A. The consistent high chargeability suggests that the rock either is weathered and/or partly altered. Since the chargeability is very high it enables the possibility that ore minerals might be present. During weathering and oxidation processes (especially if water is present) the amount of magnetite in the rock might decrease. Zone C can be referred to as “the right contact” of the dolerite dyke (Zone B) while “the left contact” would correspond to Zone A. The area between Zone C and D is composed of rock with improved quality, although fracturing probably occurs to some extent. This is based on that fact that although the resistivity is relatively low it is relatively homogenous.

Zone D (x=473450 to x=473600 m) is a low resistive zone. This region lies under a zone which shows higher resistivity. Zone D displays high IP-effect and a substantial decrease of the magnetic field intensity can be observed in the magnetic profile. The underlying low resistive zone is interpreted as a fracture zone where probably intense clay weathering has occurred. High IP effect in combination with low resistivity is characteristics for clay weathered fracture zones. The decrease of the magnetic field intensity might be explained by oxidation processes of magnetite to hema-

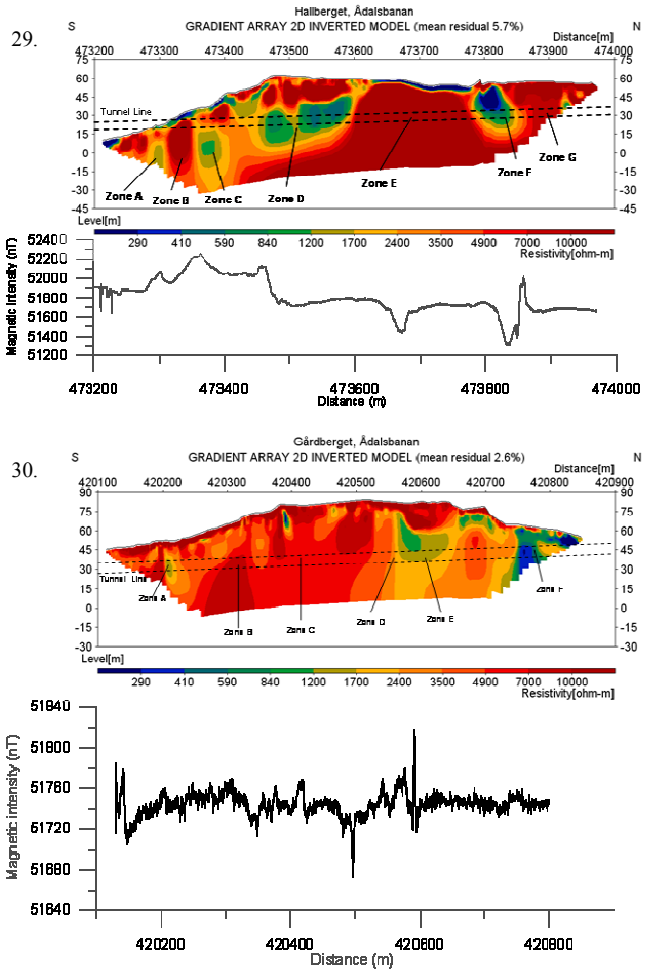

Fig. 29 & Fig. 30 Restitivity section combined with a magnetic profile and interpreted zones at Hallberget (above) and Gårdberget (below)

tite, which result in depletion of magnesium.

Zone E (x=473600 to x=473780 m) is recognised by an abrupt change in the resistivity (Fig. 29). The uppermost part consists of a layer with very low resistivities, while the underlying part is a coherent, uniform, high resistive region. It appears that the chargeability in Zone E is very low. A significant negative anomaly appears at about x=473700 m in the magnetic profile. This zone involves several significant features. The combination of results might infer that there is some kind of artefact. Since the uppermost layer is highly conductive, a large amount of the transmitted currents may be conducted laterally along this layer. In such a case the transmitted currents will not reach the underlying layer. If that is the case, the results shown above this region will not refer to the characteristics of the layer. An anomaly is apparent in magnetic profile (Fig. 29), suggesting that the layer is heterogeneous. This occurrence supports the fact that the real character of this region is obscured. If however, what is displayed in Zone E in the resistivity section is correct, it infers that the zone comprises of a solid rock. That would indicate that the rock in Zone E is of good stability and quality. Here, it might be suggested to drill, since many doubts and questions about this wide zone prevail.

Zone F (x=473780 to x=473850 m) is a low resistive subsection (Fig. 29). Here, the uppermost layer has high resistivity and chargeability. In the magnetic diagram a negative anomaly appears. All in all, Zone F is interpreted as a clay weathered fracture zone. Pegmatite dykes and aggregate of clay minerals might be present, since the chargeability is high. Zone F is assumed to cause technical difficulties during the construction, as the zone consists of unstable, brittle rock.

Zone G (x=473850 to x=473930 m) is made up of high resistive rock with low chargeability (Fig. 29). In the magnetic diagram a significant shift from low to high magnetic field intensity occurs. These characteristics implies the presence of a second dolerite dyke. The quality of the rock in Zone G is considered to be good. Throughout the rest of the magnetic diagram the intensity seems relatively stable and the chargeability is constant low. This implies that no further variation of the geology occurs within the last 150 m except for a minor fracture zone that might exist in the last part at x=473940 m with lower resistivities than the surroundings.

9.2 Gårdberget

The bedrock at Gårdberget is dominated by metagreywacke often rich in mica. Several fracture zones and

open joints occur near Gårdberget. Pegmatite dykes and minor massifs of granite are exposed near the tunnel site.

The current transmitted into the ground at Gårdberget were often relatively low. This affected the quality of the IP-data, and must be accounted for in the final evaluation. Nevertheless, there are several zones found at Gårdberget that are thought to be of geotechnical importance. In Fig. 30 a rough division of the zones (A-F) are shown, which might be important during the construction of the tunnel from a technical point of view.

In the resistivity section it is apparent that variations occur. The resistivity section can be divided into two distinctive regions. The first part extends from its initiation x=420100 to about x=420530 m and is characterised by high resistivity. This part probably comprises heterogeneous rocks. The character of the rock displayed in the section (Fig. 30) comprises many irregular variations and disseminations. Most likely the major part consists of greywacke, which in turn has great enclosures of mica and/or other mineral aggregates.

Zone A (x=420200 to x=420230 m) is a narrow low resistive part (Fig. 30). Several parts within this area have high chargeability which might infer presence of several pegmatite dykes. Only a few variations occur in the magnetic diagram. It is likely that this zone is made up of fractured rock intercalated with both pegmatite dykes (areas with high chargeability) and mica-rich lithologies/layers. Probably some fractures are partly filled with water. The quality of the rock in Zone A is expected to be poor.

Zone B (x=420290 to x=420330 m) has high resistivity but the chargeability is continuously low (Fig. 30). This narrow zone most likely consists of relatively fresh solid rock. The quality of the rock in Zone B is thought to be good with minor, or no, brittle deformation.

Zone C (x=420350 to x=420530 m) is dominated by rocks with intermediate resistivity. This part is considered to be fairly homogenous, which implies minor fracturing. The quality of the rock in Zone C is thus relatively high. This may be an appropriate spot for drilling to further investigate rock quality and rock composition that dominates this zone.

Zone D (x=420550 m) is a narrow low resistive zone (Fig. 30). Note the rise in the magnetic field intensity that appears near the zone. The remaining part of Zone D and northwards is exclusively made up of low resistive rock. It is interpreted as the contact between a homogenous rock with relatively high resistivity and a considerably more fractured rock with low resistivity. It is very likely that Zone D consists of fractures with significant clay weathering. This implication is based on the apparent high chargeability found in the Normalised IP-section (Fig. 28c).

Zone E (x=420550 to x=420750 m) has low resistivity and relatively low chargeability (Fig. 30). The appearance of the zone and its physical character suggest that zone E is a wide fracture zone. It might be filled with one or several precipitated secondary minerals. The rock volume in zone E is considered to be of poor quality, and thus unstable.

Zone F (x=420750 to x=420780 m) is mainly characterised by low resistive rocks (Fig. 30). This change might reflect that a significant change of the geology has occurred. The penetration depth in this part gradually decreases from 40 m to the surface. It should be mentioned that the landscape went from a sparse and dry forest to a more wet and dense vegetation. This appearance might reflect a distinct change in the geology, since environmental- and geological settings often are related. Unfortunately there is no magnetic data over this part. In the inverted IP section (Fig. 28b) several parts show high chargeability. In zone F the technical conditions during construction are assumed to be poor, since a major part probably is affected by clay weathering and intense fracturing.

10 Modified geological Interpretations based on investigation material from Banverket

Banverket has supported this work with pre-investigation reports including data from previous geophysical investigations (Banverket 2007, 2008b & 2008c). This material enables confirmations, discards and development of some of the ideas and suggestions presented in previous part 9. As a result, several modified interpretations and new ideas will be presented. The interpretation models from both works are combined and found in appendix C. The methods used in Banverkets pre-investigations were refraction seismic, core drilling, magnetic measurements, probing and slingram.

10.1 Hallberget

A classification and estimation of the rock condition is displayed in appendix C1. The Q-value (Q-klass) used in Banverket section, is an estimation of the quality of the rock where an increased value refers to better quality (Banverket 2008b).

In Banverkets magnetic diagram an anomaly was noted at x=473550 m which were explained by an increase of magnetite. The seismic results showed that this was a low velocity zone, which is characterizing for a weakness zone. This information seems to be contradictive, since weak zones often are characterized by a decrease of magnetite, resulting in a dip in the magnetic profile. However, the geoelectrical sections presented here suggest that this region which in this work was called zone D (Fig. 30) is a weak zone. It is therefore more likely that the increase of the magnetic field intensity is caused by presence of mafic dykes appearing relatively near the surface. A drill core was brought up at Hallberget at approximately x=473420

m (KBH1). At 35 m depth a fracture with chlorite and traces of graphite appeared. The Zone D was described as a weak zone affected by intense weathering and with possibly clay mineral occurring. Hence, the presence of chlorite is expected although the existence of graphite was useful complementary information. This zone clearly indicates on high IP which may be related to the presence of graphite, which shows that the IP-method serves with significant information.

In the section at x=473700 m the slingram measurement show an anomaly that were related to a 10 m wide seismic low velocity zone. Both here and in Banverkets magnetic measurements presence of a minor dyke or inclusions in a mafic rock at the end of the profile has been indicated (Banverket 2008c). This correlation increases the reliability of the interpretation that is based on the geoelectrical methods. At x=473700 m another drill core (KBH2) were examined. At 15 m depth, the cores were made consisted of thick clay and further down at 20 m a fracture including talc was found. This information contributes to the discussion of the high resistive and homogenous zone E in the resistivity section. More information about this zone was required in order to get a more reliable interpretation. With Banverkets additional information about this zone it is certain that a narrow weak zone is present within the interval x=473600 to x=43780 m. However, this weak zone is hidden in the resistivity section. The probable explanation of what caused this artefact in the resistivity section was discussed in the previous part (9.1). The additional data makes the interpretation and the geological model more reliable. Based on the performed resistivity measurements in this work it was suggested to drill at the same location as they actually were made. This demonstrates the geoelectrical methods should be included at an initial stage in pre-investigations of tunnel constructions.

Gårdberget 10.2

Appendix C2 also shows the interpretations (the zones A-F) for Gårdberget together with interpreted fracture zones from Banverket. As can be seen in appendix C2, by Banverket, four weak zones has been interpreted to exist within the tunnel of Gårdberget (Banverket 2007). The information about these zones is rather limited. Only one core drilling (KBH2) has been made at Gårdberget and the position is marked in the resistivity profile. The drill core verified that a prominent weak zone existed at approximately x=420850 m. The information provided by Banverket is limited and only includes the distribution of the fracture zones (Banverket 2007). Thus, no further modifications of the interpretations made in this work can be made. However, what is shown in appendix C2 is significant because it shows that only the last two of Banverkets interpreted weak zones are apparent in the resistivity section at x=420740 and x=42800 m. There is no indication of existence of weak zones at x=420250 and x=420360 m in the resistivity results. Nevertheless, existence of other weak zones has been indicated with the resistivity method. Two prominent weak zones are interpreted to exist at Gårdberget approximately x=420200 m and at x=42600 m.

11 Conclusions

The results in this work demonstrate that the resistivity and IP methods are well suitable as pre-investigation methods in sub-surface tunnel construction projects. These methods have been tested at three tunnel sites with different geology, at the Bolmen tunnel and Ådalsbanan and provided useful information. The methods give direct information of significant geological structures and their character, such as occurrence of fracture zones and weathering. Furthermore, the quality and stability of different rock volumes has been possible to estimate. The resistivity and IP methods can contribute with information equivalent to other geophysical methods but they also provide additional data not possible to retrieve by other techniques. The conclusions of this work are:

- At both Bolmen and Ådalsbanan several fracture zones and mafic dykes have been detected with the resistivity method. The existence of these was verified by data from earlier investigations.
- Resistivity measurements can provide general information about the bedrock, from which a geological model can be estimated.
- Important geotechnical information about the rock quality, weak zones and dykes has been inferred at Ådalsbanan.
- The IP method gave significant information of the character (e.g. water and clay content) of the fracture zones at both Bolmen and Ådalsbanan.
- It has been possible to approximate the depth to the bedrock with the 2-D and 3-D resistivity methods at the Bolmen tunnel. The depth to the bedrock varied between 1 and 7 m. A smaller electrode separation would have increased the resolution.
- The presence of dykes and fracture zones has further been indicated with the magnetic and VLF methods. Hence, these methods complemented the IP and resistivity methods.
- Using several geophysical methods has the advantage of giving a more complete picture of the geological conditions at the construction site
- The IP method can serve as a complement to the resistivity method and with the LUND system both types of data can be obtained fast and

efficient.

- Compared to drillings and other geophysical methods e.g. refraction seismic, the CVES is a cost efficient method giving continuous information about the changes in the rock mass conditions.

- In this work a 5 m electrode separation was applied, which gave a large depth penetration but influenced the surface near resolution of the resistivity and IP measurements.

- Low current resulted in low SNR which influenced the resolution and quality of the IP data, (mainly for one of the seven investigated lines).

12 Acknowledgements

This work would not have been completed without help and support from many involved. First of all we would like to thank our supervisors Torleif Dahlin and Berit E. Danielsen for giving us the opportunity to conduct our master thesis as a part of their work. Thank you for all the time and work you've spent for making this thesis as good as possible. Our gratitude also goes to our co supervisor Ulf Söderlund for his incredible commitment and truly support throughout this time. We are really grateful for the interest you have shown of this work and all your valuable comments on the manuscript. Thank you to all at the department of Geology for making these years memorable in so many great ways, as well lecturers as our fellow students. Special thanks goes to Dr. Anders Lind for always having your door open and always making time for answering questions and also Hans Jeppsson for introducing the science of Geophysics by giving inspiring lectures. We are also indebted to Jan Israelsson and Tommy Olsson at Banverket for really making an effort by supporting us with material and out in the field. A further thanks goes to Caj Lundquist and Patrik Lissel at Sydvatten for their involvement in this work. We would also like grant our families for encouraging us to find and develop our own interests and through life giving us inspiration. Last but not least we would like to acknowledge our respective beloved Tina Vibeke and Mattias Eriksson as they both have being incredible supportive and patience during this time.

13 References

ABEM., 2007. Instruction Manual for Terrameter SAS1000/4000. http://www.abem.se/files/upload/Manual_Terrameter.pdf 2007-11-29

Andersen, T., 1996: Sr, Nd and Pb isotopic data of the Alnö Carbonatite complex. *22nd Nordic Geological Winter Meeting*. Åbo Akademi, Turku, Finland, 8-11 January. Abstract volume, 11 pp.

Andersson, J., Söderlund, U., Cornell, D., Johansson, L., Möller, C., 1999: Sveconorwegian (-Grenvillian) deformation, metamorphism and leucosome formation in SW Sweden, SW Baltic Shield: constraints from a Mesoproterozoic granite intrusion. *Precambrian Research* 98, 151-171.

Andréasson, P.G., Rodhe, A., 1990: Geology of the Protogine Zone south of Lake Vättern, southern Sweden: a reinterpretation. *GFF* 112, 107-125.

Antal, I., Freden, C., Gierup, J., Stølen, L-K., Thunholm, B., 1998: Översiktstudie av Västernorrlands län - geologiska förutsättningar. Swedish Geological Survey. *SKB report* R-98-36, 48 pp.

Axelsson, C-L., Follin, S., 2000: Grundvattensänkning och dess effekter vid byggnation och drift av ett djupförvar. *SKB report* R-00-21, 92 pp.

Banverket., 2007: Ådalsbanan delen Härnösand-Veda. Bergprognos, Spårtunnel. KM 420+750 – 421+000. Förfrågningsunderlag 2007-04-13. *Bygghandling,* uppdrag nr 612705 13497, 4 pp.

Banverket 2008a: Järnvägsplan Bollstabruk-N Nyland. 104 pp.

Banverket., 2008b: Ådalsbanan. BOLLSTADBRUK-N NYLAND. Tunnelentreprenad. Km 473+300-477+240. *Bygghandling. Ingenjörsgeologisk prognos* (handling 13.15), dokument nr 60420-13-025-003, 29 pp.

Banverket., 2008c: Ådalsbanan. BOLLSTADBRUK-N NYLAND. Nybyggnad av enkelspår inkl bangård. Bandel 232 Km 471+300 - 483+600. *Bygghandling*. PM/ *Förundersökningsrapport berg*, dokument nr 60420-13-025-002, 22 pp.

Bergman, S., Johansson, Å., Stephens, M.B., 2004: Sveriges berggrund från urtid till nutid, scale 1:1500 000. Swedish Geological Survey Ba 76

Bingen, B., Andersson, J., Söderlund, U., Möller, C., 2008: The Mesoproterozoic from Finland to Greenland. *Episodes* 31, 29-34.

Bogdanova, S.V., Page L.M., Skridlaite, G., Taran, L.N., 2001: Proterozoic tectonothermal history in the western part of the East European Craton: 40Ar/39Ar geochronological constraints. *Tectonopysics* 339, 39-66.

Brander, L., Söderlund, U., 2008: Mesoproterozoic (1.47-1.44 Ga) orogenic magmatism in Fennoscandia; Baddeleyite U-Pb dating of a suite of massif-type anorthosite in S Sweden. *International Journal of Earth Sciences* DOI 10.1007/s00531-007-0281-0.

Bäckblom, G., Stanfors, R., 1986: The Bolmen Tunnel - tunnelling through the Staverhult Fault Zone. *Engineering Geology* 23, 45-57.

Cesano, D., Olofsson, B., Bagtzoglou, A.C., 2000: Parameters Regulating Groundwater Inflows into Hard Rock Tunnels-a Statistical Study of the Bolmen Tunnel in Southern Sweden. *Tunnelling and Underground Space Technology* 15, 153-165.

Dahlin, T., 1996: 2D resistivity surveying for environmental and engineering applications. *First Break* 14, 275-283.

Dahlin, T., Bjelm, L., Svensson, C., 1996: Resistivity preinvestigations for the railway tunnel through Hallandsås, Sweden. *Procs. 2nd Eurpean EEGS Meeting*, Nantes, France, 2-4 September 1996, 109-112.

Dahlin, T., Zhou, B., 2002: Gradient and Mid-point-referred measurements for multi-channel 2D resistivity imaging. *Procs. 8th Meeting Enviromental and Engineering Geophysics*, Aveiro, Portugal, 8-12 September 2002, 157-160.

Dahlin, T., Zhou, B., 2004: A numerical comparison of 2D resistivity imaging with ten electrode arrays. *Geophysical Prospecting* 52, 379-398.

Dahlin, T., Zhou, B., 2006: Multiple-gradient array measurements for multichannel 2D resistivity imaging. *Near surface Geophysics*, 113-123.

Danielsen, B.E., 2007: The applicability of geoelectrical imaging as a tool for construction in rock. Engineering Geology. Lund University, 13 pp.

Didriksson, V., Isander, A., 1995: Collapse of the Bolmen water supply tunnel, 1995. *Sydkraft consult AB*, 5 pp.

Freden, C., 2002: Berg och Jord. Sveriges National atlas, ISBN-91-87760-50-9, p 208.

Gierup, J., Kübler, L., Pamnert, M., Persson, M., Thunholm, B., Wahlgren, C-H., Wikman, H., 1999a: Översiktstudie av Skåne län (urbergsdelen)-geologiska förutsättningar. Swedish Geological survey. *SKB report* R-99-27, 55 pp.

Gierup, J., Johansson, R., M., Persson., Stølen, L-K., Thunholm, B., Wahlgren, C-H., Wikman, H., 1999b: Översiktstudie av Kronobergs län (urbergsdelen)-geologiska förutsättningar. Swedish Geological Survey. *SKB report* R-99-19, 53 pp.

Högdahl, K., Sjöström, H., 2001: Evidence for 1.82 Ga transpressive shearing in a 1.85 Ga granitoid in central Sweden: implications for the regional evolution. *Precambrian research* 105, 37-56.

Jeppsson, H., 2006: Kompendium i Geofysiska undersökningsmetoder. Lunds Universitet. Not published.

Johansson, Å., Meier, M., Oberli, F., Wikman, H., 1992: The early revolution of the southwest Swedish gneiss province – Geochronological and isotopic evidence from southernmost Sweden. *GFF* 114, 457-458.

Johansson, L., Möller, C., Söderlund, U., 2001: Geochronology of eclogite facies metamorphism in SW Sweden. *Precambrian Research* 106, 261-275.

Klasik, J., 2006: http://geology.csupomona.edu/alert/metamorphic/mylonite.htm, 2008-03-29.

Landviser, LCC 2005: http://www.landviser.com/_vti_bin/shtml.exe/download.html, 2005-02-01.

Lantmäteriet, 2008: http://kartor.eniro.se/, 2008-08-05.

Larsson, D., Söderlund, U., 2005: Lu-Hf apatite geochronology of mafic cumulates: an example from a Fe-Ti-mineralization at Smålands Taberg, southern Sweden. *Chemical Geology* 224, 201-211.

Loke, M.H., 1997: A practical Guide to 2D and 3D surveys. Resistivities of some common rocks, minerals and chemicals, 61 pp. http://www.heritagegeophysics.com/images/lokenote.pdf

Loke, M.H., 2003: Tutorial: 2D and 3D electrical imaging surveys, 134 pp.

Lundqvist, T., Gee, D.G., Kumpulainen, R., Karis, R., Kresten, P., 1990: Beskrivning till berggrundskartan över Västernorrlands län. Swedish geological Survey Ba 31, 429 pp.

Möller, C., Söderlund, U., 1997: Age constraints on the regional deformation within the Eastern Segment, S Sweden: Late Sveconorwegian granite dyke intrusion and metamorphic-deformational relations. *GFF* 119, 1-12.

Möller, C., Andersson, J., Lundqvist, I., Hellström, F., 2007:

Linking deformation, migmatite formation and zircon U-Pb geochronology in polymetamorphic orthogneisses, Sveconorwegian Province, Sweden. *Journal of Metamorphic Geology*, 25, 727–750.

Nabighian, M.N., Grauch, V.J.S., Hansen, R.O., LaFehr, T.R., Li, Y., Peirce, J.W., Phillips, J.D., Ruder, M.E., 2005: 75th Anniversary – The historical development of the magnetic method in exploration. *Geophysics* 70, 33-61.

Nilsson, K.P., Bergman, T., Lundin, I.A., Wedmark, M., 2006: Sundsvall, berg och bergkvalitet. Swedish geological Survey, *rapporter och meddelanden* 123, 143-154.

Olofsson, B., Bjarnason, B., Gustafson, G., Leijon, B., Stanfors, R., Wallman, S., 1988: The Bolmen Tunnel Research Project, Final Report. *BeFo* 160:2, 100 pp.

Olofsson, B., 1991: Impact on groundwater conditions by tunneling in hard crystalline rocks. Department of Land and Water recourses-royal institute of technology, Stockholm, Sweden. ISBN 91-7170-068-4, p 165.

Parasnis, D.S., 1986: Principles of Applied Geophysics fourth editions. Chapman and Hall Ltd, London, ISBN 0-412-28320-4, p 402.

Reynolds, J.M., 1997: An Introduction to Applied and Environmental Geophysics. John Wiley & Sons Ltd, West Sussex., England. ISBN-13 978 04 71 96802 3, p 796.

Rowland, F.R.G., 2007: http://www.nga.com/Geo_ser_DC_tech.htm. 2008-08-08.

Sharma, P.V., 1976: Geophysical methods in geology. Elsevier Scientific publishing company, Amsterdam, ISBN 0-44-41235-2, p 428.

Slater L. D., Lesmes D., 2002: IP interpretation in environmental investigations. *Geophysics* 67, 77-88.

Stanfors, R., 1987: The Bolmen tunnel project. Evaluation of geophysical site investigation methods. *SKB technical report*, 52 pp.

Söderlund, U., Persson, P-O., Jarl, L-G., Stephens, M.B., Wahlgren, C-H., 1999: Protolith ages and timing of deformation in the eastern, marginal part of the Sveconorwegian orogen, southwestern Sweden. *Precambrian Research* 94, 29-48.

Söderlund, U., Isachsen, C., Bylund, G., Heaman, L., Patchett. P.J., Vervoort, J.D., Andersson, U.B., 2005: U-Pb baddeleyite ages and Hf, Nd isotope chemistry constraing repeated mafic magmatism in the Fennoscandian Shield from 1.6 to 0.9 Ga. *Contributions to Mineralogy and Petrology* 150, 174-194.

Söderlund, U., Ask. R., 2006: Mesoproterozoic bimodal magmatism along the Protogine Zone, S Sweden: three magmatic pulses at 1.56, 1.22 and 1.205 Ga, and regional implications. *GFF* 128, 303-310.

Söderlund U., Karlsson C., Johansson L., Larsson K., 2008: The Kullaberg peninsula – a glimpse of the Protorezoic evolutionof SW Fennoscandia. *GFF* Report, 10 pp.

Wik, N.G., Bergström, U., Claeson, D., Hellström, F., Juhojuntti, N., Jönberger, J., 2006: Berggrunds geologisk undersökning. Sammanfattning av pågående verksamhet. Swedish Geological Survey, *rapporter och meddelanden* 123, 155–196.

Åhäll, K.I., Connelly, J.N., 2008: Long-term convergence along SW fennoscandia: 330m.y. of proterozoic crustal growth. *Precambrian Research* 161, 452-474.

Dictionary

Amphibolite facies = A metamorphic regime corresponding to intermediate temperature and pressure conditions (hornblende is a characteristic mineral)

Anatexis = Partial or complete melting of rocks in the lithosphere

Aquifer = A body of permeable rock, that is capable of storing significant quantities of water and is underlain by a impermeable layer

Breccia = is a rock composed of angular fragments of rocks or minerals in a matrix, which is a cementing material that may be similar or different in composition to the fragments. A breccia may have a variety of different origins, the ones existing in the Bolmen tunnel is so called fault breccias. Fault breccias result from the grinding action between two fault blocks as they slide past each other. Subsequent cementation of these broken fragments may occur by means of mineral matter introduced by groundwater.

Electrolyte= A material or a compound that contain dissolved ions and thus is able to conduct electrical currents

Facies (metamorphic) = A range of pressure-temperature conditions characterized by specific mineral assemblages

Gabbro = A plutonic rock of mafic composition and corresponding compositionally to basalt

Greywacke = Type of sandstone marked by quartz and feltspars in a clay matrix

Granitoid = (Granitic rock) Quarts-bearing phaneritic felsic rock

Isolator= A material with low electrical conductivity

Leucratic = a rock that is rich in light minerals. Definition < 10% dark minerals e.g. biotite

msl =Meters above Sea Level

Megachrysts= a term that describe a mineral greater in size than minerals in the groundmass

Metamorphism= When a rock is transformed due high temperature and pressure.

Micas = A group of phyllosilicates (sheet silicates) with a 2:1 atomic structure and include minerals as muscovite, biothite, phlogopite

Migmatite = A mixed rock, generally with light and dark bands, due to partial melting at high grade metamorphic conditions

Mylonitization = Involves the chemical processes of metasomatism and recrystallization. In these, as well as in the deformation processes, fluids are important. Other variables that control the

nature of the mylonitization include the nature of the protolith, confining pressure, temperature, and continuity of the rock mass

Ophitic texture= Physical character that is typical for a diabase. Plagioclase crystals enclosed by larger pyroxene crystals.

Orogen = An orogenic- or mountain belt, that is produced where an oceanic plate converges against an overriding continental plate. The process usually involves folding, faulting and regional metamorphism

Phaneritic = Texture in which grains og major rock-forming minerals are all large enough to be identifiable without magnification

Phanorezoic= A geological time era, Cambrian to present time

Pegmatite = Rocks of highly variable grain size in which individual crystals can be as much as several m. A simple pegmatite consists of albite, quarts, perthite and possible minor muscovite, tourmaline and Fe-Mn garnet

Pregrouting= A thin mortar used to fill cracks and crevices in masonry. It is performed to reduce water conductivity and to stabilise a rock tunnel.

Protorezoic= A geological time era, ca 2.5-0.57 Ga

Satellite intrusion = minor intrusions that are related (i.e. similar chemical composition and ca. age) to an larger intrusion

Skarn = rocks that consists of calcium-, magnesium-, and ironrich silicate minerals as amphiboles, pyroxens and garnets as frequently occurs together with some iron- and sulphur ores (skarn ores).

Tonalite = an oversaturated, coarse-grained, igneous rock consisting of essential Na- plagioclase, quartz, hornblende, biotite and a accessory minerals

Tuff = Rock made of ash-size volcanic clasts

Volatile elements = Components in the gas phase of a magma, normally water and carbon dioxide.

Appendices

Appendix A – Inversion parameters

2-D Inversion parameters

Initial damping factor (0.01 to 1.00)
0.1600
Minimum damping factor (0.001 to 0.75)
0.0150
Line search option (0=Never, 1=Sometimes, 2=Always)
2
Convergence limit for relative change in RMS error in percent (0.1 to 20)
5.0000
Minimum change in RMS error for line search in percent (0.5 to 100)
0.4000
Number of iterations (1 to 30)
5
Vertical to horizontal flatness filter ratio (0.25 to 4.0)
1.0000
Model for increase in thickness of layers (0=default 10, 1=default 25, 2=user defined)
2
Number of nodes between adjacent electrodes (2 or 4)
2
Flatness filter type, Include smoothing of model resistivity (0=model changes only,1=directly on model)
0
Reduce number of topographical datum points? (0=No,1=Yes. Recommend leave at 0)
0
Carry out topography modeling? (0=No,1=Yes)
1
Type of topography trend removal (0=Average,1=Least-squares,2=End to end)
1
Type of Jacobian matrix calculation (0=Quasi-Newton, 1=Gauss-Newton, 2=Mixed)
1
Increase of damping factor with depth (1.0 to 2.0)
1.0500
Type of topographical modeling (0=None, 1=No longer supported so do not use, 2=uniform distorted FEM, 3=underwater, 4=damped FEM, 5=FEM with inverse Swartz-Christoffel)
0
Robust data constrain? (0=No, 1=Yes)
1
Cutoff factor for data constrain (0.0001 to 0.1))
0.0500
Robust model constrain? (0=No, 1=Yes)
1
Cutoff factor for model constrain (0.0001 to 1.0)
0.0050
Allow number of model parameters to exceed datum points? (0=No, 1=Yes)
1
Use extended model? (0=No, 1=Yes)
0
Reduce effect of side blocks? (0=No, 1=Slight, 2=Severe, 3=Very Severe)
2
Type of mesh (0=Normal,1=Fine,2=Finest)
0
Optimise damping factor? (0=No, 1=Yes)
0
Time-lapse inversion constrain (0=None,1=Least-squares,2=Smooth,3=Robust)
0
Type of time-lapse inversion method (0=Simultaneous,1=Sequential)
0
Thickness of first layer (0.25 to 1.0)
0.5000
Factor to increase thickness layer with depth (1.0 to 1.25)
1.1000
USE FINITE ELEMENT METHOD (YES=1,NO=0)

0
WIDTH OF BLOCKS (1=NORMAL WIDTH, 2=DOUBLE, 3=TRIPLE, 4=QUADRAPLE, 5=QUINTIPLE)
1
MAKE SURE BLOCKS HAVE THE SAME WIDTH (YES=1,NO=0)
1
RMS CONVERGENCE LIMIT (IN PERCENT)
1.000
USE LOGARITHM OF APPARENT RESISTIVITY (0=USE LOG OF APPARENT RESISTIVITY, 1=USE RESISTANCE VALUES, 2=USE APPARENT RESISTIVITY)
0
TYPE OF IP INVERSION METHOD (0=CONCURRENT,1=SEQUENTIAL)
0
PROCEED AUTOMATICALLY FOR SEQUENTIAL METHOD (1=YES,0=NO)
0
IP DAMPING FACTOR (0.01 to 1.0)
0.100
USE AUTOMATIC IP DAMPING FACTOR (YES=1,NO=0)
0
CUTOFF FACTOR FOR BOREHOLE DATA (0.0005 to 0.02)
0.00300
TYPE OF CROSS-BOREHOLE MODEL (0=normal,1=halfsize)
0
LIMIT RESISTIVITY VALUES(0=No,1=Yes)
1
Upper limit factor (10-50)
50.000
Lower limit factor (0.02 to 0.1)
0.020
Type of reference resistivity (0=average,1=first iteration)
0
Model refinement (1.0=Normal,0.5=Half-width cells)
1.00
Combined Combined Marquardt and Occam inversion (0=Not used,1=used)
0
Type of optimisation method (0=Gauss-Newton,2=Incomplete GN)
0
Convergence limit for Incomplete Gauss-Newton method (0.005 to 0.05)
0.005
Use data compression with Incomplete Gauss-Newton (0=No,1=Yes)
0
Use reference model in inversion (0=No,1=Yes)
0
Damping factor for reference model (0.0 to 0.3)
0.01000
Use fast method to calculate Jacobian matrix. (0=No,1=Yes)
1
Use higher damping for first layer? (0=No,1=Yes)
0
Extra damping factor for first layer (1.0 to 100.0)
2.50000
Type of finite-element method (0=Triangular,1=Trapezoidal elements)
0
Factor to increase model depth range (1.0 to 5.0)
1.000
Reduce model variations near borehole (0=No, 1=Yes)
0
Factor to control the degree variations near the boreholes are reduced (2 to 100)
5.0
Factor to control variation of borehole damping factor with distance (0.5 to 5.0)
1.0
Floating electrodes survey inversion method (0=use fixed water layer, 1=Incorporate water layer into the model)
0
Resistivity variation within water layer (0=allow resistivity to vary freely,1=minimise variation)
1
Use sparse inversion method for very long survey lines (0=No, 1=Yes)
0
Optimize Jacobian matrix calculation (0=No, 1=Yes)

0
Automatically switch electrodes for negative geometric factor (0=No, 1=Yes)
1
Force resistance value to be consistant with the geometric factor (0=No, 1=Yes)
0
Shift the electrodes to round up positions of electrodes (0=No, 1=Yes)
0

3-D Inversion parameters
Initial damping factor
0.1500
Minimum damping factor
0.0110
Line search option
1
Convergence limit
5.0000
Minimum change in RMS error
0.2000
Number of iterations
6
Number of iterations to recalculate Jacobian matrix
10
Vertical to horizontal flatness filter ratio
1.0000
X horizontal flatness filter weight
1.0000
Y horizontal flatness filter weight
1.0000
Flatness filter weight for half-size layers
1.0000
Number of nodes between adjacent electrodes
2
Normalise potentials
0
Flatness filter type, Include smoothing of model resistivity
1
Increase of damping factor with depth
1.0500
Type of topographical modeling
0
Factor for damped topography model
0.50
Type of topography trend removal
0
Robust data constrain?
0
Cutoff factor for data constrain
0.0500
Robust model constrain?
0
Cutoff factor for model constrain
0.0100
Reduce effect of side blocks?
1
Optimise damping factor?
0
Thickness of first layer
0.7000
Factor to increase thickness layer with depth
1.1500
Number of half-size layers
0
Divide half-size layers vertically (1=YES,0=NO)
0
Factor to increase model depth range
1.00

USE FINITE ELEMENT METHOD (YES=1,NO=0)
0
RMS CONVERGENCE LIMIT (IN PERCENT)
5.000
USE LOGARITHM OF APPARENT RESISTIVITY (0=LOG OF APP. RESIS., 1=RESISTANCE, 2=APP. RESIS.)
0
TYPE OF IP INVERSION METHOD (0=CONCURRENT,1=SEQUENTIAL)
1
PROCEED AUTOMATICALLY FOR SEQUENTIAL METHOD (1=YES,0=NO)
1
IP DAMPING FACTOR
0.250
USE AUTOMATIC IP DAMPING FACTOR (YES=1,NO=0)
0
CUTOFF FACTOR FOR LOW POTENTIALS (0.0005 to 0.02)
0.00200
LIMIT RESISTIVITY VALUES(0=No,1=Yes)
1
Upper limit factor (10-50)
50.000
Lower limit factor (0.02 to 0.1)
0.020
Type of reference resistivity (0=average,1=first iteration)
0
Type of optimisation method (0=Gauss-Newton,2=Incomplete GN)
2
Convergence limit for Incomplete Gauss-Newton method
0.010
Use data compression with Incomplete Gauss-Newton (0=No,1=Yes)
0
Use reference model in inversion (0=No,1=Yes)
0
Damping factor for reference model
0.20000
Type of initial model (0=Homogeneous,1=approx.inverse)
0
Time-lapse inversion constrain
0
Type of time-lapse inversion method
0
Type of time reference model,0=first,1=preceding
0
Reduce effect of side blocks? (0=No,1=Yes)
1
Use higher damping for first layer? (0=No,1=Yes)
0
Extra damping factor for first layer
2.00000
Automatically re-sort data points (0=No, 1=Yes)
1
Automatically switch electrodes for negative geometric factor (0=No, 1=Yes)
0
Automatically force apparent rsistivity values to be positive (0=No, 1=Yes)
0
Scale Incomplete Gauss-Newton method (0=No, 1=Yes)
0
Type of scaling for Incomplete Gauss-Newton method (1=First, 1=Second)
1
Use uniform filter weights (0=No, 1=Yes)
0

Appendix B - Tunnel mapping, Staverhult and Killeberg

B1. Staverhult

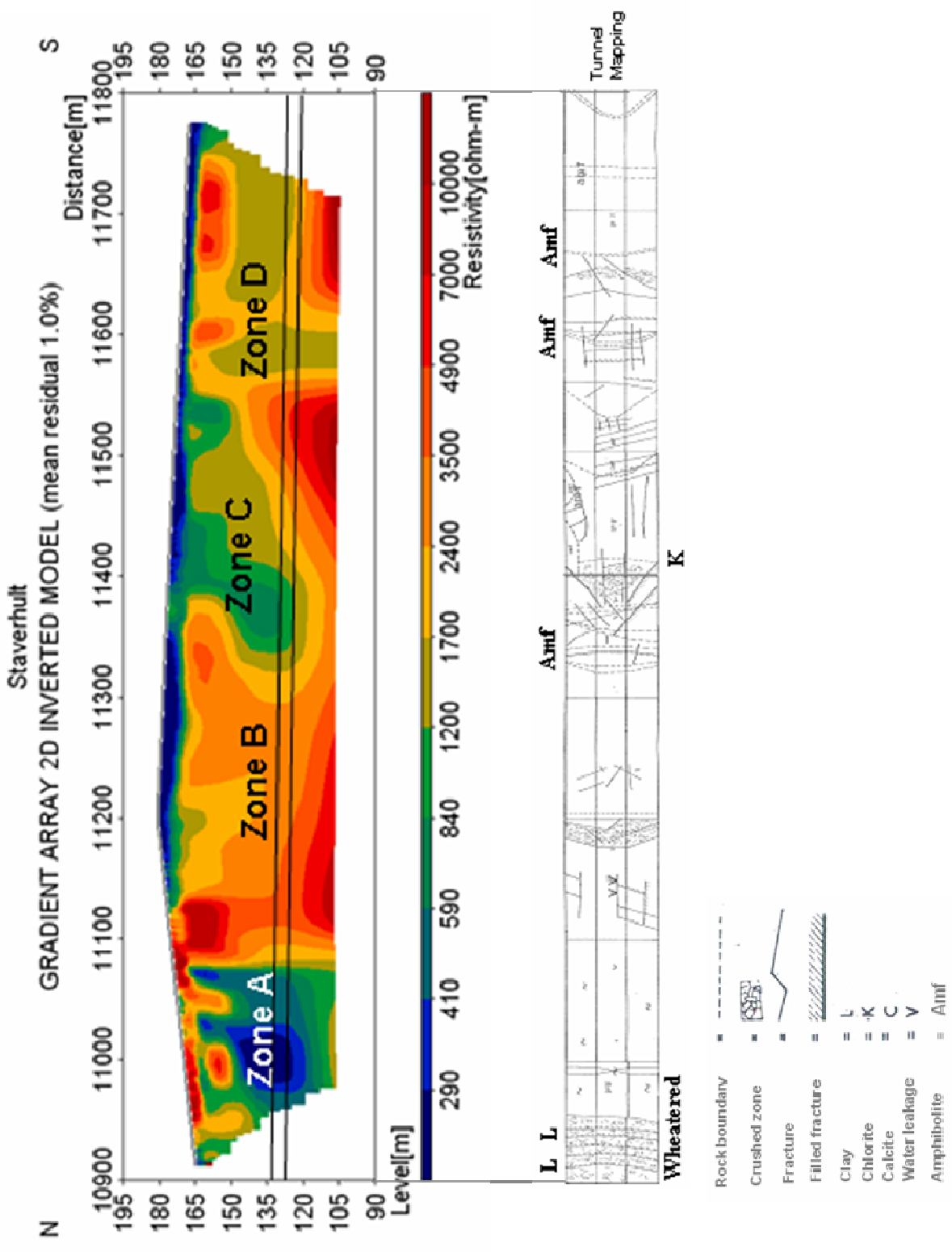

B2. Killeberg

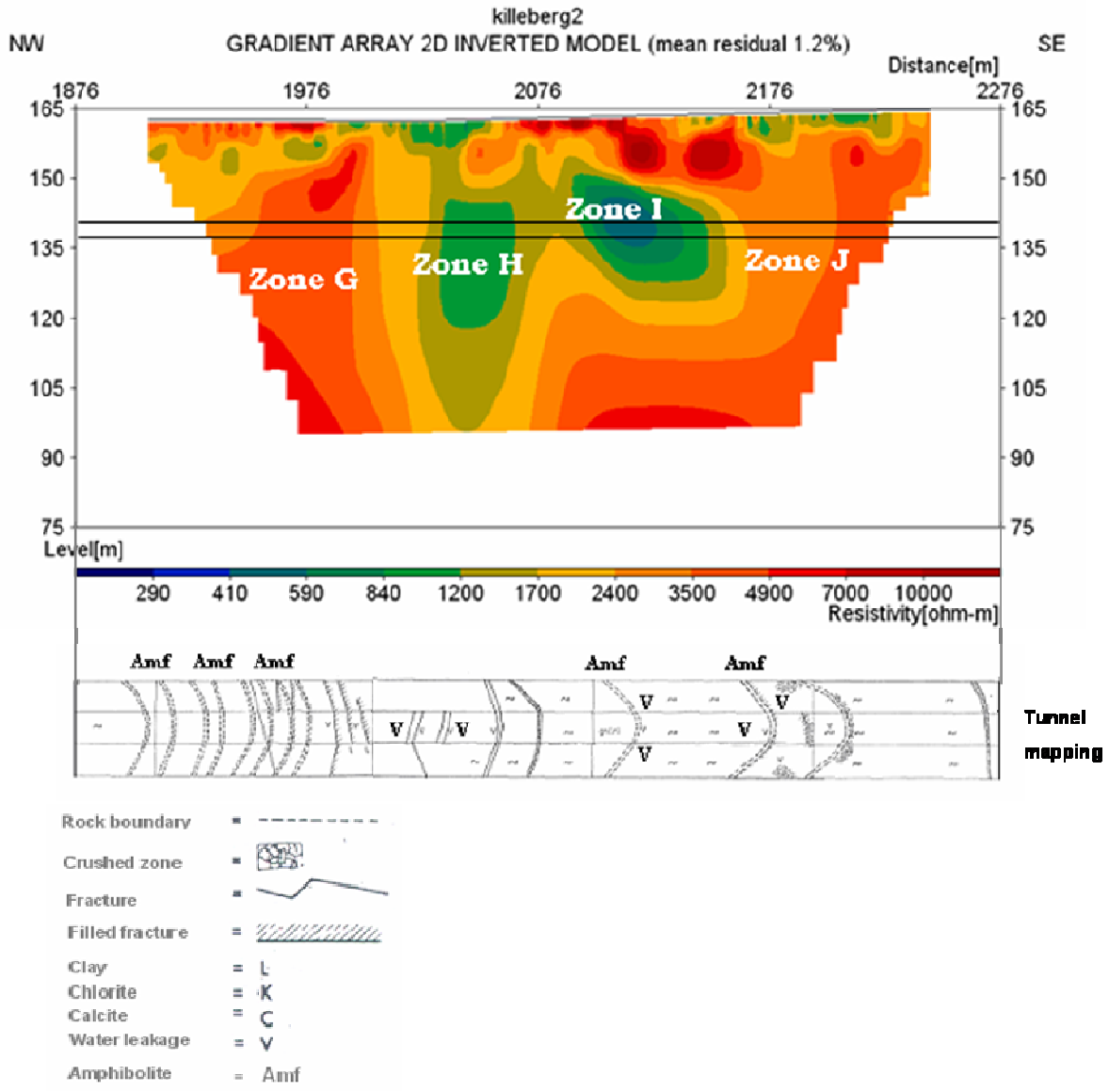

Appendix C - Results combined with drilling cores and rock quality estimations from Banverket

C1. Hallberget

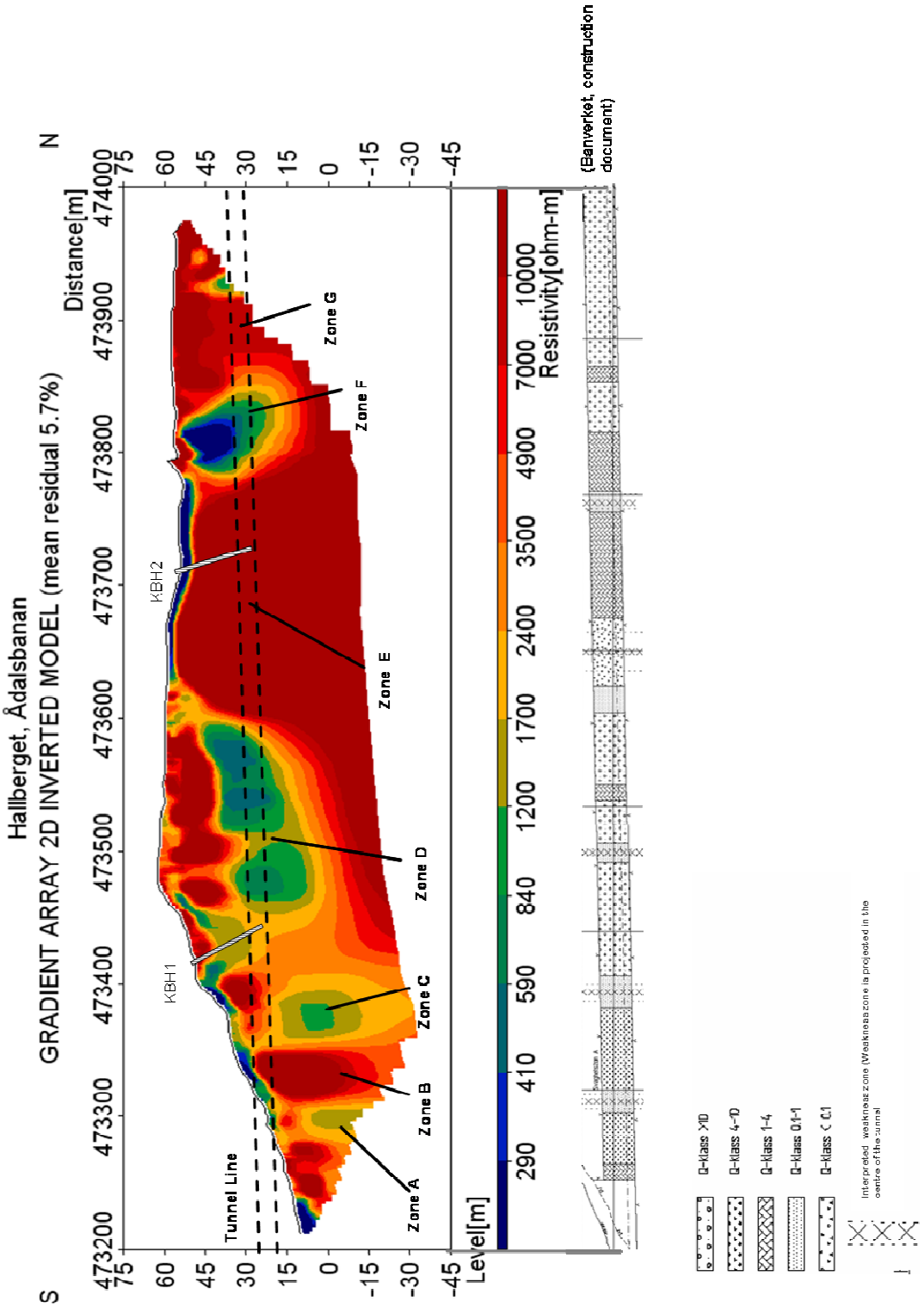

C2. Gårdberget

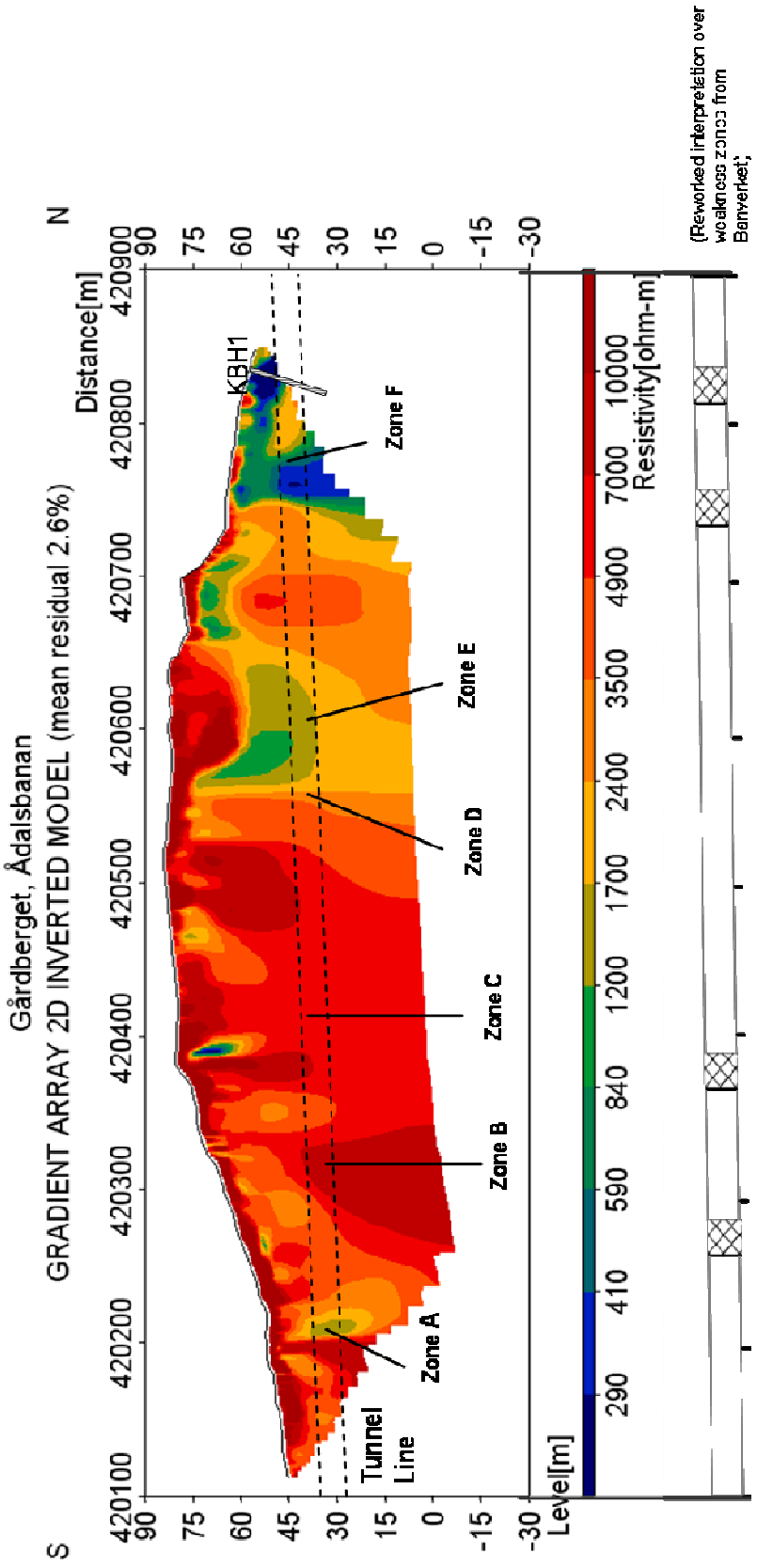

Tidigare skrifter i serien "Examensarbeten i Geologi vid Lunds Universitet":

183. Bragée, Petra, 2005: A palaeoecological study of Holocene lake sediments above the highest shoreline in the province of Västerbotten, northeast Sweden.
184. Larsson, Peter, 2005: Palynofacies och mineralogi över krita-paleogengränsen vid Stevns Klint och Kjølby Gaard, Danmark.
185. Åberg, Lina, 2005: Metamorphic study of metasediment from the Kangilinaaq Peninsula, West Greenland.
186. Sidgren, Ann-Sofie, 2005: $^{40}Ar/^{39}Ar$-geokronologi i det Rinkiska bältet, västra Grönland.
187. Gustavsson, Lena, 2005: The Late Silurian Lau Event and brachiopods from Gotland, Sweden.
188. Nilsson, Eva K., 2005: Extinctions and faunal turnovers of early vertebrates during the Late Silurian Lau Event, Gotland, Sweden.
189. Czarniecka, Ursula, 2005: Investigations of infiltration basins at the Vomb Water Plant – a study of possible causes of reduced infiltration capacity.
190. G³owacka, Ma³gorzata, 2005: Soil and groundwater contamination with gasoline and diesel oil. Assessment of subsurface hydrocarbon contamination resulting from a fuel release from an underground storage tank in Vanstad, Skåne, Sweden.
191. Wennerberg, Hans, 2005: A study of early Holocene climate changes in Småland, Sweden, with focus on the '8.2 kyr event'.
192. Nolvi, Maria & Thorelli, Gunilla, 2006: Extraterrestrisk och terrestrisk kromrik spinell i fanerozoiska kondenserade sediment.
193. Nilsson, Andreas, 2006: Palaeomagnetic secular variations in the varved sediments of Lake Goœci¹¿, Poland: testing the stability of the natural remanent magnetization and validity of relative palaeointensity estimates.
194. Nilsson, Anders, 2006: Limnological responses to late Holocene permafrost dynamics at the Stordalen mire, Abisko, northern Sweden.
195. Nilsson, Susanne, 2006: Sedimentary facies and fauna of the Late Silurian Bjärsjölagård Limestone Member (Klinta Formation), Skåne, Sweden.
196. Sköld, Eva, 2006: Kulturlandskapets förändringar inom röjningsröseområdet Yttra Berg, Halland - en pollenanalytisk undersökning av de senaste 5000 åren.
197. Göransson, Ammy, 2006: Lokala miljöförändringar i samband med en plötslig havsyteförändring ca 8200 år före nutid vid Kalvöviken i centrala Blekinge.
198. Brunzell, Anna, 2006: Geofysiska mätningar och visualisering för bedömning av heterogeniteters utbredning i en isälvsavlagring med betydelse för grundvattenflöde.
199. Erlfeldt, Åsa, 2006: Brachiopod faunal dynamics during the Silurian Ireviken Event, Gotland, Sweden.
200. Vollert, Victoria, 2006: Petrografisk och geokemisk karaktärisering av metabasiter i Herrestadsområdet, Småland.
201. Rasmussen, Karin, 2006: En provenansstudie av Kågerödformationen i NV Skåne – tungmineral och petrografi.
202. Karlsson, Jonnina, P., 2006: An investigation of the Felsic Ramiane Pluton, in the Monapo Structure, Northern Moçambique.
203. Jansson, Ida-Maria, 2006: An Early Jurassic conifer-dominated assemblage of the Clarence-Moreton Basin, eastern Australia.
204. Striberger, Johan, 2006: En lito- och biostratigrafisk studie av senglaciala sediment från Skuremåla, Blekinge.
205. Bergelin, Ingemar, 2006: $^{40}Ar/^{39}Ar$ geochronology of basalts in Scania, S Sweden: evidence for two pulses at 191-178 Ma and 110 Ma, and their relation to the breakup of Pangea.
206. Edvarssson, Johannes, 2006: Dendrokronologisk undersökning av tallbestånds etablering, tillväxtdynamik och degenerering orsakat av klimatrelaterade hydrologiska variationer på Viss mosse och Åbuamossen, Skåne, södra Sverige, 7300-3200 cal. BP.
207. Stenfeldt, Fredrik, 2006: Litostratigrafiska studier av en platåformad sand- och grusavlagring i Skuremåla, Blekinge.
208. Dahlenborg, Lars, 2007: A Rock Magnetic Study of the Åkerberg Gold Deposit, Northern Sweden.

209. Olsson, Johan, 2007: Två svekofenniska graniter i Bottniska bassängen; utbredning, U-Pb zirkondatering och test av olika abrasionstekniker.
210. Erlandsson, Maria, 2007: Den geologiska utvecklingen av västra Hamrångesynklinalens suprakrustalbergarter, centrala Sverige.
211. Nilsson, Pernilla, 2007: Kvidingedeltat – bildningsprocesser och arkitektonisk uppbyggnadsmodell av ett glacifluvialt Gilbertdelta.
212. Ellingsgaard, Óluva, 2007: Evaluation of wireline well logs from the borehole Kyrkheddinge-4 by comparsion to measured core data.
213. Åkerman, Jonas, 2007. Borrkärnekartering av en Zn-Ag-Pb-mineralisering vid Stenbrånet, Västerbotten.
214. Kurlovich, Dzmitry, 2007: The Polotsk-Kurzeme and the Småland-Blekinge Deformation Zones of the East European Craton: geomorphology, architecture of the sedimentary cover and the crystalline basement.
215. Mikkelsen, Angelica, 2007: Relationer mellan grundvattenmagasin och geologiska strukturer i samband med tunnelborrning genom Hallandsås, Skåne.
216. Trondman, Anna-Kari, 2007: Stratigraphic studies of a Holocene sequence from Taniente Palet bog, Isla de los Estados, South America.
217. Månsson, Carl-Henrik & Siikanen, Jonas, 2007: Measuring techniques of Induced Polarization regarding data quality with an application on a test-site in Aarhus, Denmark and the tunnel construction at the Hallandsås Horst, Sweden.
218. Ohlsson, Erika, 2007: Classification of stony meteorites from north-west Africa and the Dhofar desert region in Oman.
219. Åkesson, Maria, 2008: Mud volcanoes - a review. (15 hskp)
220. Randsalu, Linda, 2008: Holocene relative sea-level changes in the Tasiusaq area, southern Greenland, with focus on the Ta1 and Ta3 basins. (30 hskp)
221. Fredh, Daniel, 2008: Holocene relative sea-level changes in the Tasiusaq area, southern Greenland, with focus on the Ta4 basin. (30 hskp)
222. Anjar, Johanna, 2008: A sedimentological and stratigraphical study of Weichselian sediments in the Tvärkroken gravel pit, Idre, west-central Sweden. (30 hskp)
223. Stefanowicz, Sissa, 2008: Palynostratigraphy and palaeoclimatic analysis of the Lower - Middle Jurassic (Pliensbachian - Bathonian) of the Inner Hebrides, NW Scotland. (15 hskp)
224. Holm, Sanna, 2008: Variations in impactor flux to the Moon and Earth after 3.85 Ga. (15 hskp)
225. Bjärnborg, Karolina, 2008: Internal structures in detrital zircons from Hamrånge: a study of cathodoluminescence and back-scattered electron images. (15 hskp)
226. Noresten, Barbro, 2008: A reconstruction of subglacial processes based on a classification of erosional forms at Ramsvikslandet, SW Sweden. (30 hskp)
227. Mehlqvist, Kristina, 2008: En mellanjurassisk flora från Bagå-formationen, Bornholm. (15 hskp)
228. Lindvall, Hanna, 2008: Kortvariga effekter av tefranedfall i lakustrin och terrestrisk miljö. (15 hskp)
229. Löfroth, Elin, 2008: Are solar activity and cosmic rays important factors behind climate change? (15 hskp)
230. Damberg, Lisa, 2008: Pyrit som källa för spårämnen – kalkstenar från övre och mellersta Danien, Skåne. (15 hskp)
331. Cegrell, Miriam & Mårtensson, Jimmy, 2008: Resistivity and IP measurements at the Bolmen Tunnel and Ådalsbanan, Sweden. (30 hskp)

LUNDS UNIVERSITET

Geologiska institutionen
Gentrum för GeoBiosfärsvetenskap
Sölvegatan 12, 223 62 Lund